UNIVERSITY OF THESSALY

SCHOOL OF ENGINEERING

DEPARTMENT OF MECHANICAL ENGINEERING

Master Thesis

SIMULATION OF THE HUMAN PASSIVE THERMOREGULATION SYSTEM

by

MICHAIL MOURATIDIS

Submitted for the Partial Fulfillment

of the Requirements for the Degree of

Diploma in Mechanical Engineering

2009

Certified by the members of the Thesis Committee:

First Member (Supervisor)	Dr. Valougeorgis Dimitrios Professor, Department of Mechanical Engineering, University of Thessaly
Second Member	Dr. Bontozoglou Vasileios Professor, Department of Mechanical Engineering, University of Thessaly
Third Member	Dr. Pantelis Dimitrios Associate Professor, Department of Mechanical Engineering, University of Thessaly

Ευχαριστίες

Η ολοκλήρωση της παρούσας διπλωματικής εργασίας οφείλεται σε μεγάλο βαθμό στη βοήθεια και την καθοδήγηση του επιβλέποντα καθηγητή μου Δρ. Βαλουγεώργη Δημήτριο. Οφείλω να ομολογήσω ειλικρινώς πως οποιαδήποτε στιγμή χρειάστηκε ήταν παρών. Είμαι ευτυχής που είχα την ευκαιρία να συνεργαστώ μαζί του διότι είναι από τους λίγους ανθρώπους που γνωρίζω των οποίων ο λόγος και η πειστική συλλογιστική μού προκαλεί διαρκή θαυμασμό, σεβασμό, εμπιστοσύνη. Θα ήθελα, ακόμη, να αναφέρω πως η εργασία αυτή δε θα είχε διαμορφωθεί εάν δεν δεχόμουν τη θερμή φιλοξενία από το Ινστιτούτο Μεταφορών του Εθνικού Κέντρου Έρευνας και Τεχνολογικής Ανάπτυξης και δεν συναντούσα τον κ. Ιωάννη Συμεωνίδη ο οποίος με μεγάλη προθυμία με φιλοξένησε και μου πρότεινε το εν λόγω θέμα. Η υποστήριξή του, η στάση του σαν φίλος, οι γνώσεις του και οι συζητήσεις που είχαμε μου ανοίγουν νέους ορίζοντες. Επίσης, θα ήθελα να ευχαριστήσω τα δύο μέλη της εξεταστικής επιτροπής κκ. Μποντόζογλου Βασίλειο και Παντελή Δημήτριο που αφιέρωσαν χρόνο για την ανάγνωση της διπλωματικής μου εργασίας και για τις χρήσιμες υποδείξεις αυτών.

Θα ήθελα, ακόμα, να ευχαριστήσω τους γονείς μου Γιάννη και Αντιγόνη για την αμέριστη καθημερινή στήριξή τους όπως και τα αδέρφια μου Δέσποινα και Κωνσταντίνο για την κατανόηση και τη βοήθειά τους. Τέλος, οφείλω να αναγνωρίσω την δύναμη και την ενέργεια που πήρα από τους φίλους στους οποίους υπολόγισα καθημερινά αλλά και σε περιόδους πίεσης και συναισθηματικής φόρτισης. Ανταποκρίθηκαν με τρόπο που μόνο αυτοί γνωρίζουν δίνοντάς μου τη θέληση να προχωρήσω στο επόμενο βήμα κάθε φορά.

SIMULATION OF THE HUMAN PASSIVE THERMOREGULATION SYSTEM

MOURATIDIS MICHAIL

University of Thessaly, Department of Mechanical Engineering, 2019

Supervisor: Dr. Valougeorgis Dimitris, Professor, Department of Mechanical Engineering, University of Thessaly

Abstract

People, nowadays, most of the times are looking to an environment in which they feel thermally comfortable. Houses, commercial buildings, airplanes, trains, etc. widely use thermal comfort standards in order to provide a friendly environment to the user. The significance of pleasant thermal sensation has been highly recognized in the construction and transportation industries. For example thermal comfort in automobiles is of major importance in reducing traffic collisions, while in motorcycles thermal satisfaction is more difficult to be achieved, especially under hot and cold weather conditions.

In order to achieve thermal comfort in humans, a deeper understanding of the human passive thermoregulation system is needed and the present thesis is focusing on this issue. First, the most well-known thermal comfort models are reviewed and the so-called Fiala model is selected to be implemented in this work. Then, the human body is simulated as several human body elements which are composed of human tissue layers and are further spatially separated into sectors. The introduced physical properties are the realistic ones and are obtained from the literature based on experimental data and observations. All the passive system mechanisms contributing to the human body heat transfer and heat exchange with the surroundings are considered. These mechanisms include conduction within the human body, metabolic heat production, blood circulation, convection, long and short wave radiation, evaporation and respiration.

Furthermore, the governing equations of the human passive system are described and included in the computer model, in Matlab, which is solved based on a finite difference scheme using the implicit Crank Nicholson method. Finally, two benchmark tests are successfully carried out and two single body elements, namely the head and the neck, are simulated providing physically justified results.

ΠΡΟΣΟΜΟΙΩΣΗ ΑΝΘΡΩΠΙΝΟΥ ΠΑΘΗΤΙΚΟΥ ΣΥΣΤΗΜΑΤΟΣ ΘΕΡΜΟΡΡΥΘΜΙΣΗΣ

Μουρατίδης Μιχαήλ

Πανεπιστήμιο Θεσσαλίας, Τμήμα Μηχανολόγων Μηχανικών, 2019

Επιβλέπων Καθηγητής: Δρ. Βαλουγεώργης Δημήτριος, Καθηγητής, Τμήμα Μηχανολόγων Μηχανικών, Πανεπιστήμιο Θεσσαλίας

Περίληψη

Οι άνθρωποι, στις μέρες μας, προκειμένου να αισθάνονται ικανοποίηση δαπανούν αρκετό χρόνο ή χρήμα βελτιώνοντας τις θερμικές συνθήκες του περιβάλλοντος χώρου, στοχεύοντας στην θερμική τους άνεση. Πρότυπα θερμικής άνεσης χρησιμοποιούνται ευρέως σε εσωτερικούς χώρους σπιτιών, εμπορικών κτιρίων, αεροπλάνων, τρένων, κτλ. με σκοπό να προσφέρουν στο χρήστη ένα φιλικό περιβάλλον. Η αυτοκινητοβιομηχανία έχει αναγνωρίσει το γεγονός πως η θερμική άνεση του οδηγού είναι σημαντική στην κατεύθυνση της μείωσης των τροχαίων δυστυχημάτων. Όμως, για τους μοτοσικλετιστές παραμένει ένα δύσκολο προς επίλυση πρόβλημα, ιδιαίτερα στην οδήγηση υπό ψυχρές ή θερμές συνθήκες περιβάλλοντος.

Προς επίτευξη του στόχου αυτού απαιτείται βαθύτερη κατανόηση της θερμικής άνεσης του ανθρώπινου σώματος και η παρούσα εργασία στοχεύει στη κατεύθυνση αυτή. Αρχικά πραγματοποιείται μια βιβλιογραφική ανασκόπηση και κατηγοριοποιούνται τα υπάρχοντα μοντέλα θερμικής άνεσης. Μεταξύ των διαθεσίμων θερμικών μοντέλων επιλέγεται το μοντέλο του Fiala επειδή οδηγεί σε αξιόπιστα αποτελέσματα με σχετικό μικρό υπολογιστικό φορτίο.

Το ανθρώπινο σώμα προσομοιώνεται ως κυλινδρικά ή σφαιρικά μέλη τα οποία αποτελούνται από διαδοχικά ομοαξονικά ή ομοκεντρικά κελύφη αντίστοιχα τα οποία αναπαριστούν τους διαδοχικούς ιστούς των μελών. Η προσομοίωση και η ιδιότητες που χρησιμοποιούνται βασίζονται σε ρεαλιστικά δεδομένα που είναι αποτέλεσμα της έρευνας του Fiala. Όλοι οι μηχανισμοί του ανθρώπινου παθητικού συστήματος που συντελούν στην μετάδοση θερμότητας εντός του ιστού και την ανταλλαγή θερμότητας με το περιβάλλον μελετώνται και παρουσιάζονται. Οι εν λόγω μηχανισμοί περιλαμβάνουν αγωγή εντός του ανθρώπινου ιστού, μεταβολισμό, κυκλοφορικό σύστημα, συναγωγή, ακτινοβολία υψηλής και χαμηλής συχνότητας, εξάτμιση και αναπνοή.

Οι εξισώσεις που διέπουν τους μηχανισμούς του ανθρώπινου παθητικού συστήματος μελετώνται, περιγράφονται και συμπεριλαμβάνονται σε ένα υπολογιστικό μοντέλο σε Matlab που επιλύεται με τη μέθοδο των πεπερασμένων διαφορών εφαρμόζοντας το πεπλεγμένο σχήμα Crank Nicholson. Επιλύονται δύο πρότυπα προβλήματα και επιβεβαιώνεται η ακρίβεια του υπολογιστικού μοντέλου. Στη συνέχεια προσομοιώνονται δύο μεμονωμένα ανθρώπινα μέλη, το κεφάλι και ο λαιμός και τα αποτελέσματα που προκύπτουν θεωρούνται αποδεκτά και ακριβή.

Table of Contents

List of Tables

List of Figures

1 Introduction

1.1 Human thermal comfort

There is an unceasing effort of people to live in a comfortable thermal environment. While people is relaxing, socializing, working or even driving they are always in pursuit of thermal comfort. In several activities, thermal comfort is directly connected to public safety issues. For example in driving the vulnerability is higher when there is thermal discomfort and therefore it is of great concern.

A contributing factor to the person's comfort that needs not to be neglected is thermal comfort. By thermal comfort we mean the well-functioning state of the mind emanating from the satisfaction with surrounded thermal environment [8]. Human body is able to function into a limited range of temperatures between 36 to 38 ^{o}C. Temperature difference of five degrees in the body temperature may cause serious problems, while ten degrees difference may even cause death [2]. The human body temperature balance depends on the temperature of the surrounding environment, the air speed, the level of humidity and the radiative heat gained or lost. Furthermore, individual characteristics such as age, height, body fat and physical fitness level can attribute to the amount of heat loss or gain which can result to difficulties in maintaining comfort body temperatures [2]. In extreme conditions, is vital for the proper functioning of the mind and the human organs, to maintain the body temperature between 36-38 ^{o}C. The thermoregulatory system accounts for the complex reactions of a human body being activated to maintain body temperature and so it influences largely the thermal sensation. It appears that the temperatures within the body play a significant role on the functionality of the thermoregulatory system [10]. As a result, an in depth analysis of both the heat exchange

between human-environment and the heat transfer within the human body is mandatory so as to provide a better perspective on how human thermoregulatory system works and under which circumstances is being activated.

Automotive industry has also taken comfortable driving under serious consideration over the last decades. The purpose of the involvement in the thermal comfort during driving by automotive industry is to provide improved services and satisfaction to the costumer as well as to achieve safer driving experience. It has been noticed that the level of the careful observation and attentiveness of a driver after one hour of public road driving at surrounding temperature of 27^{o}C is significantly lower compared to one of 21 ^{o}C [26]. Especially in Motorcycle Industry where the driver's exposition to the environmental conditions is notable, the impact of thermal comfort on the driving behavior is even greater and the need to address this issue is urgent.

Given the necessity of the thermal comfort to be assessed some clearly defined standards of thermal comfort for indoor spaces, such as ANSI/ASHRAE Standard 55 and the European Standard EN15251, have been established. There are two main methods to evaluate the thermal sensation of indoor occupants: the first one is the predicted mean vote and predicted percentage of dissatisfied (PMV/PPD) model and the second one is the Adaptive model. The PMV/PPD model is used for indoor spaces that are sealed from the outdoor environment (e.g., air-conditioned spaces). With this model only one combination of temperature, humidity, radiant temperature etc. is implemented throughout the year. On the contrary, the Adaptive model is used mainly in naturally conditioned buildings and spaces where current weather conditions may have a greater impact on the indoor conditions (e.g., spaces with freely opening and closing windows) [21]. The Adaptive model takes under consideration physiological, psychological and behavioral factors to result in a level of acceptability in current conditions. It is

characteristic that the Adaptive model results in a greater range of seasonal conditions and temperatures than those resulted from the PMV/PPD model.

In order to improve human thermal comfort it has been decided that an effective computational tool is needed. This tool should be able to calculate the temperatures of a human body including the core temperature, the temperature of hypothalamus, the outer skin temperature, as well as the temperature distribution across the whole human body. Towards this effort, several models have been developed and are available in the literature.

Closing this introductory section it is noted that the author of this thesis had the opportunity to participate at the Hellenic Institution of Transportation (HIT-CERTH) in a non-funded project related to the thermal comfort of motorcycle drivers. This effort was part of a larger European Union project, namely the Adaptive Advanced Driver-Assistance Systems (ADAS&ME) project focusing on the development of an interactive system between the rider and the current weather characteristics to increase comfort and safety of the rider in long journeys.

1.2 Basic understanding of human heat exchange

Body internal and outer skin temperatures, depend on the heat flux taking place between the human and the surrounding environment. There are four main mechanisms contributing the heat transferred:

- Convection
- Radiation
- Evaporation
- Conduction

- Respiration

These mechanisms compose the so-called human passive system.

When the metabolic heat production is not balanced with the heat losses the human thermoregulatory system is activated. Human body has developed nature effective mechanisms so that it can sustain greater range of environmental conditions. The human thermoregulation comprises of the following mechanisms:

- Vasodilation
- Vasoconstriction
- Sweating
- Shivering

These mechanisms are vital for temperature to be maintained within the desired range.

In additions, people, have the ability to adjust clothing based on the current environmental conditions to improve their thermal comfort.

1.3 Thesis structure and objectives

Thermal comfort tools are widely used for several situations. More commonly, such tools are used in indoor spaces of houses, business offices, warehouses, or even cars. However, in outdoor spaces, such as in motorcycling, the situation becomes more complicated. In general, there is a growing industrial interest in thermal comfort applications.

In this framework the topic of the present diploma thesis is human thermoregulation modeling. The thesis structure is outlined as follows:

- In Chapter 1 an introduction on human thermal comfort is provided and its importance in various human activities is argued. A short description of existing standards assessing thermal comfort is written explaining the reasons clarifying that further research work is needed. Some information about the basic mechanisms that govern the heat exchange between a human being and the environment is given. The chapters of the thesis are outlined.
- In Chapter 2 the literature review is presented. The ANSI/ASHRAE 55 Standard referring to thermal comfort is described. Also, a review of the available models that concern the thermal comfort assessment is carried out following a chronological progress of the conducted research. A classification of the existing models is carried out describing the basic characteristics of each model. Then, the thermal model introduced by Fiala in 1999, which is implemented in the present work is described. Finally, a reference is made to the universal thermal comfort index (UTCI).
- In Chapter 3 the passive system of the Fiala Model used in this present work is described in detail. The mechanisms, the parameters and the equations in continuous form that govern both the heat transfer within the human body tissue and the heat exchange between the human body and the environment are analytically presented.
- In Chapter 4 the discretization of the equations based on a finite difference scheme and more specifically on the Crank Nicolson method is formulated. The boundary conditions are also discretized and explained. The mesh construction method and the equations applied to each node are considered.
- In Chapter 5 a verification of the present work is carried out by comparing results of the present work with corresponding results available in the papers by Fiala. Furthermore,

results for two individual elements of the human body, namely the head and the neck are reported.

- In Chapter 6 some concluding remarks and suggestions concerning future work are made.

2 Literature review

2.1 Thermal comfort ANSI/ASHRAE 55 Standard

Standards regarding human thermal comfort are certainly needed. One of the common standards that has been an acceptable thermal environment is the ANSI/ASHRAE 55 Standard. However, a space meeting the criteria of the standard does not necessarily indicate a universal acceptance. This is happening because the criteria are based on surveys conducted to a large group of people concerning their own thermal sensation in different indoor thermal environments and there are no specific conditions satisfying all occupants due to large individual preferences and characteristics [21].

While the ANSI/ASHRAE 55 Standard concerns indoor spaces, it is used in several applications from commercial and residential buildings to cars, trains and airplanes. There are two main methods evaluating the conditions existing in an indoor space according to the Standard. The first is the PMV/PPD model (PMV calls for Predicted Mean Vote and PPD for Predicted Percentage of Dissatisfied). The PMV is an index resulting from the mean of the votes in a survey conducted to a large group of people voting for their thermal sensation based on the ASHRAE thermal sensation scale. This scale, as shown in Figure 2.1, ranges from -3 (cold) to +3 (hot). The scale includes zero for neutral thermal sensation indicating thermal comfort. Similarly, PPD is an index representing the percentage of the voters being dissatisfied based on ASHRAE thermal sensation scale. PPD assumes that votes of ±2 and ±3 indicate dissatisfaction. As a result PPD diagram is symmetrical to 0 and neutral thermal sensation. It is notable that there is no combination of variables statistically satisfying everyone i.e. the predicted percentage of dissatisfied does not reach 0% [21].

It is characteristic that PMV/PPD Method is applied in indoor air-conditioned spaces where the impact of the weather on indoor conditions is negligible. This means all the variables such as humidity, air speed, radiant temperature and activity level have to be under control and into the range the method suggests. The method acceptable range of activity level is 1 to 1.3 *met* (1 *met* equals $58.1\,W/m^2$), which corresponds to the activity of a seated and standing person, while clothing must be from 0.5 *clo*, a typical summer clothing (1 *clo* equals $0.155\,m^2\,K/W$), to 1 *clo*, a typical winter clothing. The air speed is suggested to be less than $0.2\,m/s$. Furthermore, this method considers a whole body thermal comfort and, yet, does not take discomfort of body local parts under consideration [21]. Local discomfort can be influenced by radiant temperature asymmetries, air movement asymmetries, vertical air temperature differences, floor temperature and temperature variations with time.

The second method is the Adaptive Model and concerns the indoor spaces that are being naturally conditioned. Such spaces can be conditioned by the freely closing and opening of windows from the occupants except for mechanical ventilation which is allowed. The Adaptive Model, as it is called, concerns activity levels of 1 to 1.3 *met*, while there is not a specific range of clothing insulation, air speed and humidity. A useful conclusion made by the survey conducted for the Adaptive Model is that occupant expectations regarding the thermal sensation are different when they control the surrounding conditions, for instance by controlling the window operation, compared to when the indoor space is automatically conditioned [21].

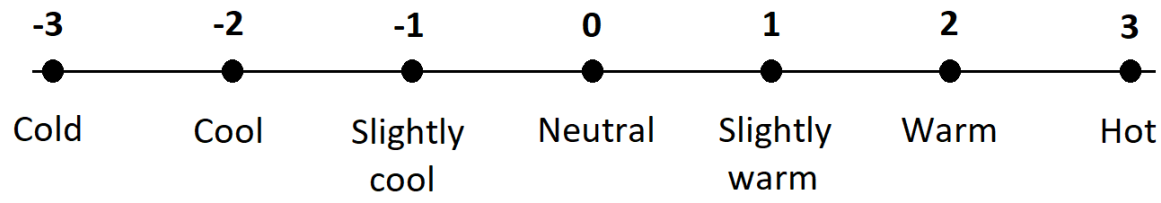

Figure 2.1 : The ASHRAE thermal sensation scale [4]

2.2 Discomfort index

For outdoor spaces a Discomfort Index (*DI*) that measures the thermal sensation of human has been proposed by Thom since 1959. Thom's Discomfort Index was used to evaluate the level of human discomfort based on the parameters of ambient air temperature and humidity [8] and is useful due to its simple formula. The formula is given by

$$DI = T - 0.55\,(1 - 0.01RH)\,(T - 14.5)\ , \tag{2.1}$$

where T is air temperature in ^{o}C and RH is the relative humidity in percentage (%). The Discomfort Index classification is shown in Table 2.1 with the higher values of DI corresponding to higher discomfort.

Classification	***DI* Values**
Uncomfortable	$DI \leq 14.9$
Comfortable	$15.0 \leq DI \leq 19.9$
Partially comfortable	$20.0 \leq DI \leq 26.4$
Uncomfortable	$DI \geq 26.5$

Table 2.1 : A classification for the discomfort index values [8].

2.3 Review and classification of thermal comfort models

Thermal comfort determination and simulation has caused concern to scientists for many decades. The history of thermal comfort is long and has been greatly influenced by the following researchers: a) the kata-thermometer found by Leonard Hill, b) the effective temperature index introduced by Houghton and Yaglou, c) the corrected effective temperature brought by Vernon and Warner, d) the wet-bulb globe temperature introduced by Yaglou and Minard introduced and e) the equivalent temperature and a correction of it found by Dufton and Gagge respectively. Furthermore, thermal comfort models have greatly influenced by the Fanger postulations. The PMV Model, used by the ASHRAE Standard until today, has been based on the conclusions made by Fanger [19].

The human thermal physiological have made the determination of thermal comfort in different situations a more complicated problem. Methodologies needed for evaluating the human thermal sensation in indoor and outdoor environments pushed scientists to conduct further research with more detailed thermal physiological models. The models are classified according to two levels: first according to the human body separation, for instance into segments, and second according to each segment separation as shown in Figure 2.2. In the first level the human body can be simulated in three ways: a) as a single-segment body, b) as a multi-segment body or c) as a multi-element body. In the second level of classification each segment is separated into: a) one-node, two-node, multi-node and multi element thermal physiological models [19], [6].

Single-segment models represent the human body as one segment or element, while multi-segment models separate it into more elements. Multi-element models simulate a three dimensional body representation using finite element analysis. Each segment can be

represented as a) uniform layer (one-node), b) two layers (two-node) and c) with multiple layers (multi-node).

A famous single-segment one-node model was introduced by Givoni and Goldman. It is an empirical model that is applied in spaces with hot conditions [6] proposing equations for metabolic costs of specific human activities [19].

The single-segment two-node models simulate the whole body as one spherical element with two concentric layers. One famous model is the Gagge model, a two-node model which represents the outer layer as the human outer skin and the inner layer as the core. Both layers appear to have the same temperature at each layer volume and it is important to mention the model is separated into two systems; a control and a controlled system [6] while the simulation includes physiological calculations for sweating, shivering, vasoconstriction and vasodilation [19]. The Gagge model can be applied in environments with uniform conditions and without extreme activity levels [6]. Another well-known two-node model is the KSU model, named after the Kansas State University, with differences in the equations regarding sweating and blood flow in comparison with the Gagge model [6]. Other two-node models have been developed and all of them simulate the human body as two concentric shells.

While many models represent the inner and outer shell as the core and the outer human skin respectively with uniform temperatures, the problem complexity requires more detailed simulations in order to obtain reliable and accurate information of the heat flux inside the human body. Such an analysis is adopted by the multi-segment multi-node models. These models represent the several human body parts as cylinders or spheres made up of many coaxial and concentric layer shells respectively [11] with a non-uniform temperature distribution within each layer. As far as the active system is concerned, every body part can have different

thermoregulatory responses based on its temperatures that enable the model to have a better estimation of the human local temperatures [19].

The first multi-node model introduced by Crosbie using the analog computer technology to perform the needed calculations [19]. Then, Stolwijk introduced a revolutionary multi-segment multi-node model [24] in thermal physiological models with passive and active systems. The human body was divided into six segments each one including four layers and regarded a uniform central blood temperature throughout the body without taking counter-current flow heat exchange under consideration. The active system is governed by the rate of temperature changes and hot or cold signals. It is notable that Stolwijk model was developed and supported by NASA aiming to simulate and predict astronaut responses. Although the Stolwijk model is restricted to steady environmental conditions, it has largely contributed to thermal comfort model progress forming the basis for many future projects [19]. The Tanabe Model, the Berkelay Model, which is based on Tanabe work [6] and the Munir et al model have been all partially based on Stolwijk approaches [19]. Multi-node models are also, the Berkley Comfort Model, the Tanabe Model, the Fiala Model, the ThermoSEM Model and others [19]. The present work is based on Fiala Model.

The most complicated models are the multi-element models. These models separate the body into several body parts where finite element or finite difference method is applied and may contain mass balances for oxygen, carbon dioxide, lactic acid and detailed simulation of the blood circulatory system, respiratory system [6]. Therefore these models are able to predict the physiological responses. However, as it is mentioned, due to their complexity memory capacity is necessary – especially when no symmetry is assumed – [19]. Most of them are computationally expensive for general purposes and they are applied when the requirement is to predict the thermal comfort of people within a specific range of individual characteristic

differences. Multi-element models are the ones introduced by Wissler, by Smith (the KSU Model), by Ferreira et al, by Schwarz et al and several others [6], [19].

Body Separation	Classification	Model
Single-Segment	One-node	Fanger 1970 Givoni and Goldman 1971
	Two-node	Gagge 1971 KSU two-node 1977
Multi-Segment	Two-node	Kohri and Mochida 2002 Crosbie 1961
	Multi-node	Stolwijk 1971 Fiala 1999 UC Berkeley 2001 Tanabe 2002 ThermoSEM 2004 Lai and Chen 2016
	Multi-element	Wissler 1985 Smith 1991 Ferreira 2009 Schwarz 2010

Table 2.2 : Classification of the most famous thermal comfort models

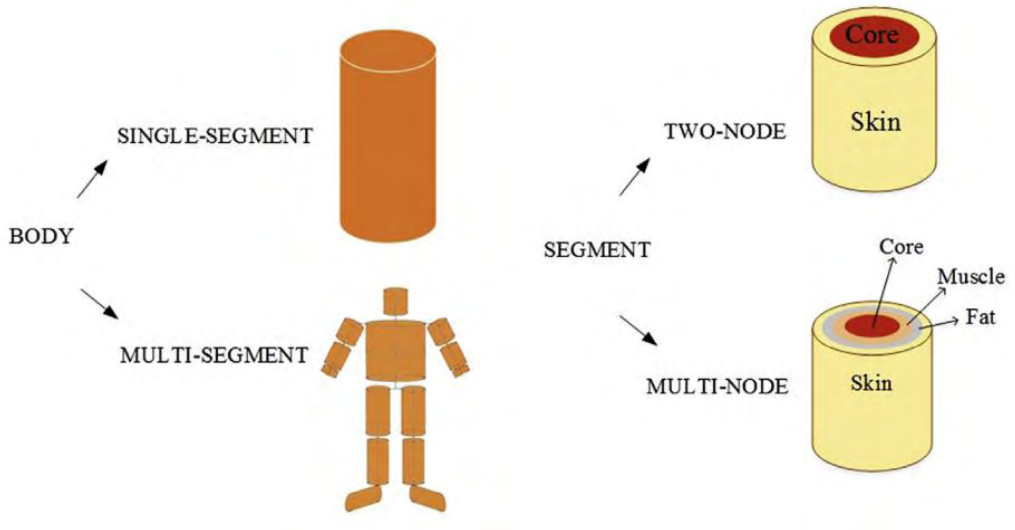

Figure 2.2 : Descriptive view of the model classification [19].

2.4 The Fiala model characteristics

The Fiala Model is a multi-segment multi-node thermal comfort model and one of the most well-known and recognized models. It is thoroughly predicted in [11] and there are also some improvements of the original model in [12], [13] . The original Fiala Model, introduced in 1999, is including an active and a passive system with blood circulation simulated. Furthermore, the Fiala Model is applicable to indoor and outdoor environments in steady or transient conditions and to a great range of activity levels, from low activity level till up to 10 *met* [10].

The active system is taking under consideration the thermoregulatory reactions of the human body; vasomotion, sweating and metabolism changes due to shivering [10]. Data for simulating the active system have been obtained with regression analysis of experiment data, given in Table 2.3. The analysis showed that the thermo-physiological reactions are influenced by the skin temperature, hypothalamus temperature and the rate of skin temperature changes. Based on the physiological effects the predicted percentage of dissatisfied (PPD) can be calculated, while a dynamic thermal sensation has also been developed [10].

The passive system refers to the heat transfer by conduction within the human body, by convection due to blood circulation and the heat exchange with the environment. The human body is separated into fifteen cylindrical and spherical body parts each separated into sectors in order to better apply the non-uniform environmental conditions. In a following improvement of the model the human body parts are further broken down to 20 [13]. At each sector a 1D heat transfer problem is solved with the finite difference method and all 1D problems are then coupled via the blood circulation throughout the body [10].

In the present work it has been decided to implement the original Fiala model with the 15-elements because it combines reasonable computational effort with reliable results. Also, only the passive system is considered.

2.5 The Universal Thermal Climate Index

European Union has created a European Program called COST Action 730 a part of which funds the development of a Universal Thermal Climate Index, the so-called UTCI. The term universal refers to the range of the outdoor thermal conditions assessed. Its main purpose is to carry out an assessment of the conditions of an outdoor thermal environment [3]. The UTCI approach is to develop an equivalent temperature at which a reference environment of 50% relative humidity, still air and the mean radiant temperature equaling the air temperature would cause equivalent physiological responses with the actual environment [3].

It is notable that among all the human thermoregulation models evaluated one of the most appropriate model is found to be the Fiala model. Some of the conducted research has been focused on simulating the clothing insulation of the general public as function of the environmental conditions. More specifically, it has been considered how clothing insulation is distributed to the body resulting to a local clothing insulation model and how this insulation is influenced during walking by the relative speed of air [3]. These developments are providing tools that are adjusted to be working well with the Fiala Model.

The UTCI, finally, aims to be established as an international standard that could have the potential to be useful in several disciplines and fields such as bio-meteorology, weather services, health systems, urban planning, tourism and others.

Passive System Parameters (Fiala Model)

Body Elements	L (cm)	h_x (W/K)	$h_{c,mix}$			a_{sk}	$a_{m,w}$		Sector	φ	ψ		ε_{sf}	Tissue Material	N	r (cm)	k W/(m K)	ρ (kg/m^3)	c J/(kg K)	$q_{m,bas,0}$ (W/m^3)	$w_{bl,0}$ l/(s m^3)
			a_{nat}	a_{frc}	a_{mix}	[-]	Sed	Stnd		[°]	Sed	Stnd									
Head	-	0.00	3.0	113	-5.7	0.0835	0.00	0.00	Forehead	10	1.00	1.00	0.99	Brain	5	8.60	0.49	1080	3850	10.1320	13400
									Head	170	0.90	0.90	0.80	Bone	2	10.05	1.16	1500	1591	0.0000	0
														Fat	2	10.20	0.16	850	2300	0.0036	58
														Skin	4	10.40	0.47	1085	3680	5.4800	368
Face	9.84	0.00	3.0	113	-5. 7	0.0418	0.00	0.00		210	0.90	0.90	0.99	Muscle	1	2.68	0.42	1085	3768	0.5380	684
														Bone	1	5.42	1.16	1500	1591	0.0000	0
														Muscle	1	6.80	0.42	1085	3768	0.5380	684
														Fat	2	7.60	0.16	850	2300	0.0036	58
														Skin	2	7.80	0.47	1085	3680	11.1700	368
Neck	8.42	0.00	1.6	130	-6.5	0.0417	0.03	0.01	Anterior	180	0.70	0.70	0.99	Bone	1	1.90	0.75	1357	1700	0.0000	0
									Posterior	180	0.75	0.75	0.99	Muscle	4	5.46	0.42	1085	3768	0.5380	684
														Fat	2	5.56	0.16	850	2300	0.0036	58
														Skin	4	5.67	0.47	1085	3680	6.8000	368
Shoulders	32.00	0.80	5.9	216	-10.8	0.0300	0.05	0.02		130	0.90	0.90	0.99	Bone	1	3.70	0.75	1357	1700	0.0000	0
														Muscle	2	3.90	0.42	1085	3768	0.5380	684
														Fat	2	4.40	0.16	850	2300	0.0036	58
														Skin	2	4.60	0.47	1085	3680	1.0100	368
Thorax	30.60	0.00	0.5	180	-7.4	0.3060	0.12	0.07	Anterior	150	0.80	0.90	0.99	Lung	1	7.73	0.28	550	3718	CO	600
									Posterior	150	0.95	0.95	0.99	Bone	3	8.91	0.75	1357	1700	0.0000	0
									Inferior	60	0.05	0.10	0.99	Muscle	3	12.34	0.42	1085	3768	0.5380	684
														Fat	6	12.68	0.16	850	2300	0.0036	58
														Skin	6	12.90	0.47	1085	3680	1.5800	368
Abdomen	55.20	0.00	1.2	180	-9.0	0.1210	0.46	0.20	Anterior	150	0.80	0.90	0.99	Viscera	1	7.85	0.53	1000	3697	4.3100	4100
									Posterior	150	0.95	0.95	0.99	Bone	3	8.34	0.75	1357	1700	0.0000	0
									Inferior	60	0.20	0.30	0.99	Muscle	3	10.90	0.42	1085	3768	0.5380	684
														Fat	6	12.44	0.16	850	2300	0.0036	58
														Skin	6	12.60	0.47	1085	3680	1.4400	368
Arms	127.40	4.13	8.3	216	-10.8	0.1800	0.19	0.08	Anterior	135	0.75	0.85	0.99	Bone	1	1.53	0.75	1357	1700	0.0000	0
									Posterior	135	0.80	0.90	0.99	Muscle	3	3.43	0.42	1085	3768	0.5380	684
									Inferior	90	0.10	0.20	0.99	Fat	6	4.01	0.16	850	2300	0.0036	58
														Skin	6	4.18	0.47	1085	3680	1.1000	368
Hands	62.00	0.57	8.3	216	-10.8	0.0900	0.02	0.01	Handback	180	0.80	0.80	0.99	Bone	1	0.70	0.75	1357	1700	0.0000	0
									Palm	180	0.10	0.20	0.99	Muscle	2	1.74	0.42	1085	3768	0.5380	684
														Fat	2	2.04	0.16	850	2300	0.0036	58
														Skin	4	2.26	0.47	1085	3680	4.5400	368
Legs	139.00	6.90	5.3	220	-11.0	0.2080	0.11	0.60	Anterior	150	0.85	0.90	0.99	Bone	1	2.20	0.75	1357	1700	0.0000	0
									Posterior	150	0.95	0.90	0.99	Muscle	6	4.80	0.42	1085	3768	0.5380	684
									Inferior	60	0.10	0.65	0.99	Fat	6	5.33	0.16	850	2300	0.0036	58
														Skin	6	5.53	0.47	1085	3680	1.0500	368
Feet	48.00	3.40	6.8	210	-10.5	0.0750	0.02	0.01	Instep	180	0.90	0.90	0.99	Bone	1	2.00	0.75	1357	1700	0.0000	0
									Sole	180	1.00	1.00	0.99	Muscle	2	2.50	0.42	1085	3768	0.5380	684
														Fat	4	3.26	0.16	850	2300	0.0036	58
														Skin	4	3.50	0.47	1085	3680	1.5000	368
Blood																		1069	3650		

Table 2.3 : Passive-system parameters for the Fiala Model. L: length; hx: countercurrent heat exchange coefficient; $h_{c,mix}$: heat-exchange coefficient for mixed convection; a_{nat}, a_{frc}, a_{mix}: corresponding regression coefficients, a_{sk}: skin sensitivity coefficients used for mean skin temperature; $a_{m,w}$: workload distribution coefficient, φ: sector angle; ψ: view factor between sector and the surroundings; Sed and Stnd: sedentary and standing activity, ε_{sf}: surface emission coefficient; N: no. of nodes; r: outer radius; k: heat conductivity; ρ: material density; c: heat capacitance; $w_{bl,0}$ and $q_{m,bas,0}$: basal values for blood perfusion and metabolic rates in thermal neutrality, respectively, table received from [11].

3 The human thermoregulation Fiala model: the passive system

3.1 Human body characteristics

The way a body exchanges heat with the environment and the thermoregulation reactions differ from person to person. There are thermal physiological models that can roughly predict the human body reaction and thermal comfort by calculating uniform temperatures throughout the human body. In addition, there are human thermoregulation models which are able to calculate the body core temperatures, outer skin temperatures and the temperature distribution within the tissue a more sophisticated analysis must be conducted. One of the most well-known and recognized human thermoregulation models is the Fiala Model, which simulates the human body in a pretty realistic way, taking under consideration the properties of many basic tissues of the body, with modest computational effort.

Furthermore, since the body characteristics contribute to the heat transfer mechanisms it is important to give an emphasis on how the human body is simulated. The aim is to simulate an average person and therefore the subject's overall data for the passive system are presented in Table 3.1.

Weight (kg)	***Body Fat (%)***	A_{sk} (m^2)	wt_{sk} ***(%)***	***CO (l/min)***	$M_{bas,0}$ ***(W)***
73.5	14	1.86	6	4.9	87.1

Table 3.1 : Overall data of the subject for the passive system: A_{sk} the total skin surface, wt_{sk} the wetted skin area ratio, *CO* the basal cardiac output, $M_{bas,0}$ the basal metabolism [11].

According to the Fiala Model the human body is separated, as shown in Figure 3.1, into fourteen cylindrical partitions: face, neck, thorax, abdomen and a pair of shoulders, arms, hands, legs and feet, plus one spherical: the head. In the simulation the above separation is presented with 10 elements, 9 cylindrical and 1 spherical, by just assuming the pairs of partitions as 1 element with the aggregate length. The elements may be made up of 7 different tissue materials: bone, muscle, brain, viscera, lung, fat, skin. To encounter the asymmetrical conditions around the body taking place in the heat transfer problem every element is separated in sectors. For most of the elements there are three sectors, namely the anterior, posterior and inferior sectors, while there only two sectors for the head element (head and forehead), the hand elements (handback and palm) and for the feet elements (instep and sole). The parameters of the whole passive model simulation are presented in detail in Table 2.3.

The sector separation of every element enables the model to apply different conditions and thus simulate the environment in a more realistic way. The different environmental conditions are applied through the boundary conditions of the heat transfer problem. For instance, in a case where a source in front of the body radiates heat, the anterior sectors will be influenced more compared with the hidden sector. Given that such inhomogeneous conditions are always taking place, sector separation is practically necessary.

Every element of the body is assumed to have a core with uniform temperature. The core is the first layer of each and every element. The only exception is the head element whose inner core (hypothalamus) is made up by brain tissue and has an outer radius of 4 cm which is less than the brain outer radius. Every layer following the core is presented as a coaxial cylinder shell for the cylindrical elements and concentric spherical shell for the spherical one.

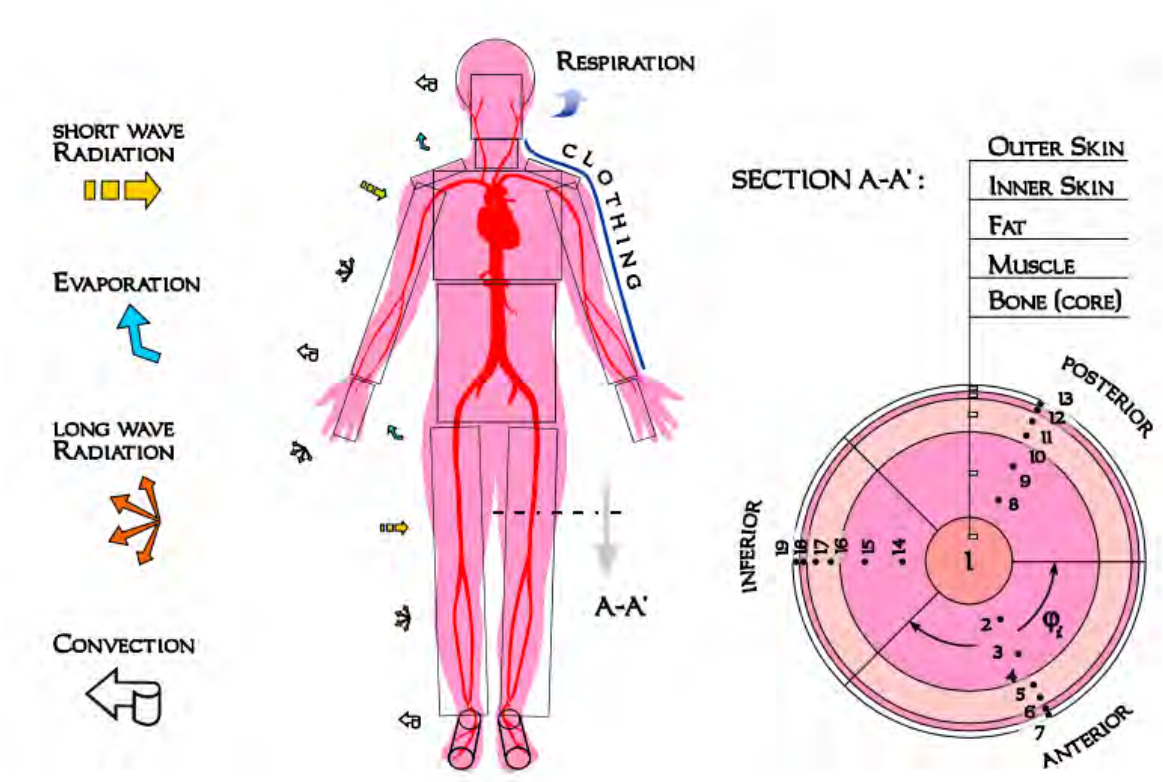

Figure 3.1 : Schematic view of human body for Fiala Model

3.2 Tissue heat transfer

The human body passive system depends on the heat transferability of the human tissue. Pennes introduced a differential equation which describes the heat transfer within a single tissue, named the "bioheat equation" which is formed as [11]

$$\rho c \frac{\partial T}{\partial t} = k\left(\frac{\partial^2 T}{\partial r^2} + \frac{\omega}{r}\frac{\partial T}{\partial r}\right) + q_m + \rho_{bl} w_{bl} c_{bl}\left(T_{bl,a} - T\right), \tag{3.1}$$

where $T\ \left(^{o}C\right)$ is the unknown tissue temperature, r is the radius (m), t is the time (s), ω is a geometry factor equal to 1 for cylindrical coordinates or 2 for spherical, $k\ \left(W/(m\,K)\right)$ is the thermal conductivity, $\rho\ \left(kg/m^3\right)$ is the density, $c\ \left(J/(kg\,K)\right)$ is the heat capacity, $T_{bl,a}$ is the

arterial blood temperature, q_m $\left(W/m^3\right)$ is the tissue metabolism produced in a finite tissue volume, ρ_{bl}, w_{bl} and c_{bl} are the blood density, blood perfusion rate and blood heat capacity accordingly. It is noted that the arterial blood temperature $T_{bl,a}$ is, in general, not known and in most cases it is expressed in terms of the tissue temperatures of all body elements. It is also noted that the parameters w_{bl} and q_m are influenced by the active system and they are updated at every iteration.

3.2.1 Metabolic heat production

The human body produces heat constantly as a result of human activity and body organ functioning. It is important, at this point, to define the thermal neutral conditions for the human as presented in Fiala [11]. Thermal neutral (or thermoneutral) conditions are the environmental variables (air temperature, relative humidity, air velocity, etc.) to which a reclining unclothed subject is exposed, while no thermoregulation reactions occur [10] and the subject is in thermal comfort. These conditions are described in Table 3.2.

T_{air} (°C)	T_{mrt} (°C)	v_{air} (m/s)	RH (%)	ε_w	act_{bas} (met)
30	30	0.05	40	0.93	0.8

Table 3.2 : Environmental conditions of thermoneutral conditions: T_{air} is the air temperature, T_{mrt} is the mean radiant temperature v_{air} is the air temperature**,** RH is the relative humidity, ε_w is the wall emissivity and act_{bas} is the basal activity level [11].

The heat produced in thermo neutral conditions by a finite tissue volume regardless of the activity level is the basal metabolic heat $q_{m,bas,0}$ $\left(W/m^3\right)$ and it is given for the model for all the tissues and elements of the body in Table 2.3. Assuming that $\Delta q_m \left(W/m^3\right)$ is any

additional heat produced, the total metabolic heat production $q_m \left(W/m^3\right)$, in equation (3.1), is the summation

$$q_m = q_{m,bas,0} + \Delta q_m \,. \tag{3.2}$$

The additional heat Δq_m is a result of the activity level and the thermoregulation reactions of the body such as shivering. To be more specific, the heat produced by shivering $q_{m,sh} \left(W/m^3\right)$ and by workout $q_{m,w} \left(W/m^3\right)$ are produced only in muscle tissues, while in all other tissues are equal to zero. However, there is an additional basal metabolic heat $\Delta q_{m,bas} \left(W/m^3\right)$ which is the difference between the actual basal metabolic heat and the basal one in thermo neutral conditions is given by

$$\Delta q_m = \Delta q_{m,bas} + q_{m,sh} + q_{m,w} \tag{3.3}$$

for muscle tissues and

$$\Delta q_m = \Delta q_{m,bas} \tag{3.4}$$

for the rest of the tissues. The change in the basal metabolic heat rate is due to the changes of the human body thermal state and it is governed by the temperature coefficient Q_{10} with the value equal to 2. So, it is written as

$$Q_{10} = 2 = \left(\frac{q_{m,bas,0} + \Delta q_{m,bas}}{q_{m,bas,0}} \right)^{\frac{10}{T - T_0}} \Rightarrow \Delta q_{m,bas} = q_{m,bas,0} \left(2^{\frac{T - T_0}{10}} - 1 \right) . \tag{3.5}$$

The heat produced $q_{m,w}$ due to body movement, is not distributed uniformly in all muscles because of the difference of the activity throughout the body parts. The distribution coefficient $a_{m,w}$ expresses this heat distribution between the element muscles and is found in

Table 2.3 for sedentary and standing activity level. The heat produced due to body movement is computed as

$$q_{m,w} = \frac{\partial\left(a_{m,w}H\right)}{\partial V_{msc}} \ , \tag{3.6}$$

where $H\ \left(W\right)$ is the internal whole body workload and $V_{msc}\left(m^3\right)$ is the element muscle volume.

The internal whole body workload is the difference between the workload and the external mechanical work. Similar to every machine, human body has its own mechanical efficiency η, introduced by Fiala [11] with regression analysis as

$$\eta = 0.2\tanh(b_1\, act + b_0) \ , \tag{3.7}$$

where *act* (*met*) is the actual activity level and $b_1 = 0.39 \pm 0.13$, $b_0 = -0.60 \pm 0.28$ are regression coefficients [11]. For activity level up to 1.6 the human body efficiency is zero and rises when increasing the activity level. The internal workload due to exercise is

$$H = act\frac{M_{bas,0}}{act_{bas}}\left(1-\eta\right) - M_{bas,0} \ , \tag{3.8}$$

where $M_{bas,0}$ and act_{bas} are obtained from Table 3.1 and Table 3.2 accordingly.

3.2.2 Blood circulation

Blood supplies the element tissues with perfusion rates w_{bl} which in thermoneutral conditions is the basal perfusion rate $w_{bl,0}$, given in Table 2.3. Studies have shown that by increasing the metabolic heat q_m the perfusion rate is linearly increased [11]. For the amount of

the product $\rho_{bl} c_{bl} w_{bl}$ the Fiala Model assumes an energy equivalent β. Since the product $\rho_{bl} c_{bl}$ is constant, β rises linearly with the metabolic heat increase. The relationship between the change of the energy equivalent $\Delta\beta$ and metabolic heat Δq_m is governed by the proportionality constant $\mu_{bl} = 0.932\ (1/K)$ as [11]

$$\Delta\beta = \mu_{bl}\ \Delta q_m \tag{3.9}$$

and finally

$$\beta = \beta_0 + \Delta\beta\ , \tag{3.10}$$

where $\beta_0 = \rho_{bl} c_{bl} w_{bl,0}$.

The blood circulation within the human body is simulated in the Fiala Model. Warm blood is supplied from the blood pool to the major arteries. From the arteries the blood enters the capillary beds where most of the heat exchange with the tissues occurs. The blood is carried towards the heart via the veins and ends up to, what we call the so-called blood pool. In the heat exchange problem, the warm blood is obtained by the blood pool and while it is going to the capillary beds, it exchanges heat with the tissues in the capillary beds. In extremities and in the shoulders [11], heat is also exchanged by convection with the adjacent veins operating as a counter-current heat exchanger (CCX). This circulation is taken under consideration in the Fiala Model and it is described in detail in the following equations.

Considering any element *e*, the rate of heat loss of the arterial blood temperature that reaches the element *e* ($T_{bl,a,e}$ (^oC)), due to the CCX with the veins, equals the heat gain rate of the vein blood temperature before ($T_{bl,v}$ (^oC)) and after the CCX ($T_{bl,v,ccx}$ (^oC)). It is readily deduced that

$$\int \beta dV\,(T_{bl,p} - T_{bl,a,e}) = \int \beta dV\,(T_{bl,v,ccx} - T_{bl,v}),\ \forall e\ , \tag{3.11}$$

where $T_{bl,p}$ (^oC) is the blood pool temperature, β $\left(W/\left(m^3\,K\right)\right)$ is the blood energy equivalent of the corresponding dV $\left(m^3\right)$ finite tissue volume. The counter-current heat flow rate for every element e between arterial and vein blood is calculated as

$$\dot{Q}_x = h_x(T_{bla,e} - T_{bl,v,e}),\ \forall\ e\ , \tag{3.12}$$

where h_x is the counter-current heat transfer coefficient (W/K). Given that the model assumes that the blood after the capillary beds reaches equilibrium with the surrounding tissue it is readily deduces that

$$T_{bl,v,e} = \frac{\int \beta T\, dV}{\int \beta\, dV},\ \forall\ e\ . \tag{3.13}$$

The heat loss rate of the arterial blood that reaches the element e is equal to the CCX rate between arterial and vein blood. By combining (3.11) and (3.12)

$$\int \beta\, dV \left(T_{bl,p} - T_{bl,a,e}\right) = h_x \left(T_{bl,a,e} - T_{bl,v,e}\right),\ \forall\ e\ .$$

Then, by inserting Eq. (3.13) to the equation above and rearranging yields

$$T_{bl,a,e} = \frac{T_{bl,p} \int \beta\, dV}{h_x + \int \beta\, dV} + \frac{h_x \int \beta T\, dV}{\int \beta\, dV \left(h_x + \int \beta\, dV\right)},\ \forall\ e\ . \tag{3.14}$$

While Eq. (3.14) is valid for every element, the CCX does not occur in all elements and therefore h_x may be zero to some of them (Table 2.3).

3.3 Human-environment heat exchange

The human thermoregulation is responsible for the body temperature maintenance. For this reason the body has developed complex reactions such as shivering, sweating, etc. The heat

exchange with the surroundings is a very significant factor. In extreme conditions the body could be unable to manage to achieve the desired temperatures. Since the environmental conditions are playing an important role to human thermal comfort emphasis must be given to how a person loses or gains heat from the surroundings.

The human body exchanges heat with the environment via five mechanisms: convection, long and short wave radiation, evaporation and respiration. A practical way for a person to influence the thermal equilibrium is clothing, a factor that although it does not depend on the thermoregulation system, it must be taken under consideration. The thermal equilibrium for the human environment heat exchange is expressed to

$$q_{sk} = q_c + q_R - q_{sR} + q_e \ , \tag{3.15}$$

where $q_{sk}\ \left(W/m^2\right)$ is the net heat flux from the skin, $q_c\ \left(W/m^2\right)$, $q_R\ \left(W/m^2\right)$ and $q_e\ \left(W/m^2\right)$ are the convective, radiative and evaporative heat flux, while q_{sR} is the heat loss due to short wave radiation. All these heat transfer mechanisms are analyzed in detail in this section.

3.3.1 Convection

The convective heat flux is given by

$$q_c = h_c \left(T_{bs} - T_{air}\right) \ , \tag{3.16}$$

where $h_c\ \left(W/m^2\,K\right)$ is the convective heat transfer coefficient, T_{bs} (^oC) is the temperature of the outer face of the corresponding body sector (might be the outer cloth surface if clothes are worn) and T_{air} (^oC) the air temperature. The convective heat transfer coefficient is obtained for free and forced convection with regression analysis [13] and is given by

$$h_c = \sqrt{a_{nat}\sqrt{T_{bs} - T_{air}} + a_{frc} v_{air} + a_{mix}} \ , \tag{3.17}$$

where $a_{nat,}$ a_{frc} and a_{mix} are the resulted coefficients of the regression analysis and v_{air} is the relative local air speed.

3.3.2 Long and short wave radiation

Long wave radiation is an important way of heat exchanging, especially when the air velocity is relatively low, and it is due to the temperature difference between the human body and the surroundings. The asymmetries in the temperatures in the environment are encountered in two ways: a) by defining a mean environment temperature $T_{env,m}$ of a uniform envelope "seen" by a sector [11] which would radiate the same amount of heat with the actual heat being radiated or b) by defining a mean radiant temperature T_{mrt} which considers a uniform black envelope [11] resulting to a difference in the emissivity values. The latter approach is implemented to this present work. $T_{env,m}$ calculation process is described in [11] while the quantity T_{mrt} of a thermo neutral environment is shown in Table 3.2. The view factors for every element sector are given in Table 2.3.

The total radiative heat flux q_R is computed as

$$q_R = h_R \left(T_{bs} - T_{env,m} \right) \ , \tag{3.18}$$

where h_R the radiative heat transfer coefficient $\left(W \middle/ \left(m^2 K \right) \right)$ is

$$h_R = \sigma \varepsilon_{bs} \varepsilon_{env} \psi \left(T_{bs}^{*2} + T_{env,m}^{*\ 2} \right) \left(T_{bs}^{*} + T_{env,m}^{*} \right) \ , \tag{3.19}$$

where $\sigma = 5.67 \cdot 10^{-8}\ W/\left(m^2\ K^4\right)$ is the Stefan-Boltzmann constant, ε_{bs}, ψ are each sector emissivity and view factor respectively of each sector (both given in Table 2.3), ε_{env} is the emissivity of the surroundings and T_{bs}^{*} and $T_{env,m}^{*}$ are the body sector absolute temperature and mean environment absolute temperature all in Kelvin. The emissivity ε_{env} for the case of mean radiant temperature equals 1 (black envelop), while for the case of mean environment temperature is typically 0.93 for indoors otherwise has to be calculated [11]. The ε_{env} is typically 0.95 for clothing [11].

Heat flux via short wave radiation or irradiation q_{sR} also contributes to total heat transfer. Irradiation is emitted by high temperature surfaces and sources (e.g. sun) and is calculated by

$$q_{sR} = a_{bs}\, \psi\, s \ , \tag{3.20}$$

where a_{bs} is an absorption coefficient of the sector surface, ψ is the view factor of the body sector and environment and $s\ \left(W/m^2\right)$ is the radiant intensity which magnitude is given according to the climate characteristic.

3.3.3 Evaporation

Evaporation is the only mechanism of the human thermoregulation that allows cooling when the temperature of the environment exceeds the body temperature. It is a useful reaction which is mainly driven by the difference between the partial water vapour pressure at human skin (p_{sk} in Pa) and partial water vapour pressure of air (p_{air} in Pa), which is called the evaporative potential. The latent heat balance for each sector is given by

$$\frac{p_{sk} - p_{air}}{R_{e,lT}} = \frac{p_{s,sk} - p_{sk}}{R_{e,sk}} + \lambda_{H^2O}\, \frac{1}{A_{sk}}\, \frac{dm_{sw}}{dt} \ , \tag{3.21}$$

where the $p_{s,sk}$ is the saturated water vapour pressure (Pa) within the skin (location of sweat glands) [13], $R_{e,lT}$ $\left(\left(m^2\ Pa\right)/W\right)$ is the local evaporative resistance of clothing described in Subsection 3.3.5, $1/R_{e,sk}$ $\left(W/\left(m^2\ Pa\right)\right)$ is the human skin moisture permeability, λ_{H^2O} (J/kg) is the heat of vaporization of water, A_{sk} is the sector's skin surface (m^2) and dm_{sw}/dt (kg/s) is the sweat production rate. More specifically, the left hand side is the net energy transfer which is equal with the summation of the two terms on the right hand side of the equation representing the heat transfer by moisture diffusion (first term) and the total sweat evaporation on the skin (second term). The human skin moisture permeability is $R_{e,sk}=1000/3\ W/\left(m^2\ Pa\right)$ [11], the heat of vaporization of water is $\lambda_{H^2O}=2256\times10^3\ J/kg$, the local evaporative resistance is discussed in subsection 3.3.5 and the saturated water vapour pressure within the skin is calculated for the model according to [11]

$$p_{s,sk}=100\exp\left(18.956-\frac{4030}{T_{osk}+235}\right). \tag{3.22}$$

The calculation of the saturation value of partial water vapour pressure $p_{air,sat}$ is also presented. Although it can be calculated with several formulas, in the present work, the following equation is used [1]

$$p_{air,sat}=\frac{1}{T_{air}^{*\ 8.2}}\exp\left(77.345+0.0057\cdot T_{air}^{*}-\frac{7235}{T_{air}^{*}}\right). \tag{3.23}$$

Here T_{air}^{*} is the air temperature in Kelvin and $p_{air,sat}$ is in Pascal. Then, the actual partial water vapour pressure of air is calculated by

$$p_{air}=RH\ p_{air,sat}\ , \tag{3.24}$$

where *RH* is the relative humidity (as a decimal). Based on the above, in Eq. (3.21) for the latent heat balance, the only unknown variable is p_{sk} , which is calculated by rearranging the equation, resulting to

$$p_{sk} = \frac{\frac{p_{air}}{R_{e,lT}} + \lambda_{H^2O}\frac{1}{A_{sk}}\frac{dm_{sw}}{dt} + \frac{p_{s,sk}}{R_{e,sk}}}{\frac{1}{R_{e,lT}} + \frac{1}{R_{e,sk}}} \ . \tag{3.25}$$

It is important to mention that when sweating occurs, the pressure p_{sk} may reach its saturation value ($p_{s,sk}$). Then, the sweat starts to accumulate according to equation

$$\frac{dm_{acc}}{dt} = \frac{dm_{sw}}{dt} - \frac{A_{sk}}{\lambda_{H^2O}}\frac{\left(p_{s,sk} - p_{air}\right)}{R_{e,lT}} \ , \tag{3.26}$$

where dm_{acc}/dt is the sweat accumulation rate $\left(kg/s\right)$. It has been founded by Jones and Ogawa [11] that the accumulation of sweat stops when the amount of sweat per square meter of skin m_{acc}/A_{sk} reaches the amount of $35\,g/m^2$.

3.3.4 Respiration

For the human body heat transfer problem the heat losses due to respiration must also be included. However, they comprise only a small amount of the total heat transferred. The respiratory losses occur by convection and evaporation. The Fiala Model uses the work by Fanger, which takes under consideration both convection and evaporation for calculating the latent and dry heat losses [11] the summation of which comprise the total respiratory losses.

The latent heat losses are influenced by three factor: a) the whole body metabolism Q_m (in Watt) $\left(Q_m = \int q_m dV\right)$, because of the relationship between the ventilation rate and metabolism, b) the difference in humidity of the exhaled and inhaled air, which depends on the air temperature and partial vapour pressure and c) the latent heat of vaporization. The formula for the respiratory latent heat losses E_{rsp} (W) is [11]

$$E_{rsp} = 4.373\, Q_m \left(0.028 - 6.5\cdot 10^{-5}\, T_{air} - 4.91\cdot 10^{-6}\, p_{air}\right) . \tag{3.27}$$

The respiratory dry heat losses C_{rsp} (W) are influenced by the breathing rate, thus by the whole body metabolism and the partial vapour pressure and temperature of ambient air [11]. It is given by

$$C_{rsp} = 1.948\cdot 10^{-3}\, Q_m \left(32.6 - 0.066\, T_{air} - 1.96\cdot 10^{-4}\, p_{air}\right) . \tag{3.28}$$

For the present work both formulas are used, although in the most recent work by Fiala ([12], [13]) they have been slightly changed.

The total respiratory heat losses, which is the sum of E_{rsp} plus C_{rsp}, are then distributed to the body parts. The respiratory losses do not influence all the body elements equally, therefore by using work from within the literature it is concluded [11] that they are distributed as follows

- 30 percent in the lung
- 25 percent in the neck muscle
- 20 percent in the inner face muscles
- 25 percent in the outer face muscles

Consequently, the heat generation q_m in those tissues is calculated by

$$q_m = q_{m,bas,0} + \Delta q_m - \frac{\partial\left[a_{rsp}\left(E_{rsp} + C_{rsp}\right)\right]}{\partial V}\ , \tag{3.29}$$

where a_{rsp} are the tissue distribution coefficients for respiratory heat losses and $V\left(m^3\right)$ the corresponding tissue volume.

3.3.5 Clothing

The clothing resistances include heat transfer resistances (or thermal insulation) and evaporative resistances. Fiala made a computer model in order to construct a database for these two types of resistances for several clothes [11]. The computed resistances include the insulation effect of air trapped between clothes and skin [11]. The final expression calculates the local resistances of both types.

The total local heat transfer resistance $R_{lT}\left(m^2\ K/W\right)$ is calculated by [13]

$$R_{lT} = \sum_{i=1}^{n} R_{lcl,i} + \frac{1}{f_{cl}\left(h_c + h_r\right)}\ , \tag{3.30}$$

where $R_{lcl,i}\left(m^2\ K/W\right)$ is the local thermal resistances for the i-cloth, n is the number of the clothes for this sector, h_c and $h_R\left(W/\left(m^2\ K\right)\right)$ are the local convective and radiative heat transfer coefficients respectively and f_{cl} is a fraction in which the outer clothing layer radius r_{cl} (m) is divided by the outer skin radius r_{sk} (m) for each and every sector given by

$$f_{cl} = \frac{r_{cl}}{r_{sk}} \tag{3.31}$$

The total local evaporative resistance $R_{e,lT}$ $\left(m^2\ Pa/W\right)$ for every sector is estimated according to [13]:

$$\mathrm{R}_{e,lT} = \sum_{i=1}^{n} R_{e,lcl,i} + \frac{1}{f_{cl}\, h_e} \tag{3.32}$$

with

$$h_e = L_a h_c \ , \tag{3.33}$$

where $R_{e,lcl,i}$ $\left(m^2\ Pa/W\right)$ is the local evaporative resistance of every i-cloth and $L_a = 0.0165\, K/Pa$ is the Lewis constant for air [13].

3.4 Boundary conditions

The formulation of the boundary condition is of primary importance for every physical problem described by differential equations. The boundary conditions for the human heat transfer problem include the interface boundary condition when the tissue properties are changing i.e. at the interface between the tissue layers, the core boundary condition and the skin boundary condition for the heat transferred from the skin to the surroundings.

3.4.1 Interface

In the interface between two layers, the boundary condition is obtained by equating the heat flow rate from the one layer towards the interface $\dot{Q}_{1\to ifc}\left(W\right)$ with the heat flow rate from the interface to the second layer $\dot{Q}_{ifc\to 2}\left(W\right)$, i.e.,

$$\dot{Q}_{1\to ifc} = \dot{Q}_{ifc\to 2} \tag{3.34}$$

The heat rate within a tissue with uniform thermal conductivity *k* and a surface area of $A(r)$ in polar coordinates is

$$\dot{Q} = -k\,A(r)\frac{dT}{dr} \tag{3.35}$$

and is differently calculated for cylindrical and spherical shells. In the Appendix A the radial heat flow rates are found for cylindrical and spherical shells.

3.4.2 Core

For the core boundary condition a modified version of the Pennes bioheat equation is used. In the core no temperature gradient exists and therefore the heat conduction term is replaced by the heat fluxes $q_{ifc,s}\ \left(W/m^2\right)$ passing from the core interface to every s-sector of the element. With subscript *j* indicating the core node the bioheat equation is modified as [11]

$$\rho_j c_j \frac{dT_j}{dt} = q_{m,j} + \beta_j\left(\mathrm{T}_{bl,a} - T_j\right) - \frac{\kappa}{\pi r_j}\sum_{s=1}^{S}\varphi_s q_{ifc,s}\ , \tag{3.36}$$

where $\kappa=1$ for cylindrical elements and $\kappa = 3/2$ for the spherical element, φ_s (rad) is the angle of every s-sector, *S* is the number of sectors of each element and $q_{ifc,s}\ \left(W/m^2\right)$ are the heat fluxes calculated by the heat fluxes for cylinders or spheres as described in equations (4.17) and (4.18).

3.4.3 Skin

The skin boundary condition is very important due to the fact that it concerns the human-environment heat exchange and contains all the environmental variables. The boundary

condition results from the equality of the conductive heat flux reaching to the skin $q_{sk}\ \left(W/m^2\right)$ and the total heat flux from the skin to environment due to convection, radiation, evaporation and irradiation written as (see also in Eq. (3.15))

$$q_{sk} = q_c + q_R + q_e - q_{sR} \ .$$

By substituting all heat fluxed and rearranging the resulting equation yields to

$$q_{sk} = \frac{T_{sk} - T_o}{R_{lT}} + \frac{p_{sk} - p_{air}}{R_{e,lT}} \ , \tag{3.37}$$

where T_o (^oC) is the so-called operative temperature calculated by

$$T_o = \frac{h_c T_{air} + h_r T_{mrt} + \psi a_{bs} s}{h_c + h_r} \ . \tag{3.38}$$

4 Finite difference method analysis

The Fiala Model solves the human heat transfer model by the finite difference method (FDM) and the same approach is applied in the present work. By separating the human body into elements and sectors, the problem is simplified and for each sector a one-dimensional (1-D) problem is formulated and all problems are coupled through the blood circulation model. The simplification on the geometry of the problem, by introducing the spherical or cylindrical layers, enables the use of the FDM which may be problematic otherwise in more complex geometries due to the difficulty of analyzing the boundary conditions.

In the following paragraphs the equations composing the human heat transfer problem are approximated by the FDM. The discretized equations are explained in detail.

4.1 Tissue heat transfer

4.1.1 Pennes bioheat equation analysis

The FDM analysis is carried out by adopting the Crank Nicholson method by averaging the implicit and explicit method as [11]

$$\Omega_{CN}\, T\big|_j^t = \frac{1}{2}\left(\Omega_{ex}\, T\big|_j^t + \Omega_{im}\, T\big|_j^{t+1}\right) . \tag{4.1}$$

Assuming that the distance between nodes j and $j+1$, denoted by Δr_j, is different than the corresponding distance between $j-1$ and j nodes Δr_{j-1}, the discretization is done through the Taylor series as follows:

$$T\Big|_j^{t\pm1} = T\Big|_j^t \pm \left.\frac{\partial T}{\partial t}\right|_j^t \Delta t_t + \left.\frac{\partial^2 T}{\partial t^2}\right|_j^t \frac{{\Delta t_t}^2}{2} \pm O({\Delta t_t}^3) \tag{4.2}$$

$$T\Big|_{j+1}^t = T\Big|_j^t + \left.\frac{\partial T}{\partial r}\right|_j^t \Delta r_j + \left.\frac{\partial^2 T}{\partial r^2}\right|_j^t \frac{{\Delta r_j}^2}{2} + \left.\frac{\partial^3 T}{\partial r^3}\right|_j^t \frac{{\Delta r_j}^3}{6} + \left.\frac{\partial^4 T}{\partial r^4}\right|_j^t \frac{\Delta r_j^4}{24} + O(\Delta r_j^5) \tag{4.3}$$

$$T\Big|_{j-1}^t = T\Big|_j^t - \left.\frac{\partial T}{\partial r}\right|_j^t \Delta r_{j-1} + \left.\frac{\partial^2 T}{\partial r^2}\right|_j^t \frac{\Delta r_{j-1}^2}{2} - \left.\frac{\partial^3 T}{\partial r^3}\right|_j^t \frac{\Delta r_{j-1}^3}{6} + \left.\frac{\partial^4 T}{\partial r^4}\right|_j^t \frac{\Delta r_{j-1}^4}{24} + O(\Delta r_{j-1}^5) \tag{4.4}$$

The derivatives are formed with rearranging as follows:

$$\left.\frac{\partial T}{\partial t}\right|_j^t = \frac{T\Big|_j^{t+1} - T\Big|_j^t}{\Delta t_t} + O(\Delta t_t) \tag{4.5}$$

$$\left.\frac{\partial T}{\partial r}\right|_j^t = \frac{T\Big|_{j+1}^t - T\Big|_{j-1}^t}{\Delta r_{j-1} + \Delta r_j} + O(\Delta r) \tag{4.6}$$

$$\left.\frac{\partial^2 T}{\partial r^2}\right|_j^t = \frac{T\Big|_{j+1}^t - 2T\Big|_j^t + T\Big|_{j-1}^t}{\frac{\Delta r_{j-1}^2}{2} + \frac{\Delta r_j^2}{2}} + O(\Delta r) \tag{4.7}$$

Obviously, for $\Delta r_j = \Delta r_{j-1}$ the space discretization becomes second order. For now on, for simplicity $T\Big|_j^t$ will be denoted as T_j^t. The $\Omega_{ex} T_j^t$ and $\Omega_{im} T_j^t$ for the Pennes bioheat equation (3.1) are formed as follows:

$$\Omega_{ex} T_j^t : \rho_j c_j \frac{T_j^{t+1} - T_j^t}{\Delta t_t} = k_j \left(\frac{T_{j+1}^t - 2T_j^t + T_{j-1}^t}{\frac{\Delta r_{j-1}^2}{2} + \frac{\Delta r_j^2}{2}} + \frac{\omega}{r_j} \frac{T_{j+1}^t - T_{j-1}^t}{\Delta r_{j-1} + \Delta r_j} \right) + q_{m,j}^t + \beta_j^t \left(T_{bl,a}^t - T_j^t \right)$$

$$\Omega_{im} T_j^t : \rho_j c_j \frac{T_j^{t+1} - T_j^t}{\Delta t_t} = k_j \left(\frac{T_{j+1}^{t+1} - 2T_j^{t+1} + T_{j-1}^{t+1}}{\frac{\Delta r_{j-1}^2}{2} + \frac{\Delta r_j^2}{2}} + \frac{\omega}{r_j} \frac{T_{j+1}^{t+1} - T_{j-1}^{t+1}}{\Delta r_{j-1} + \Delta r_j} \right) + q_{m,j}^{t+1} + \beta_j^{t+1} \left(T_{bl,a}^{t+1} - T_j^{t+1} \right)$$

Finally, the discretized Pennes bioheat equation for the Crank Nicholson scheme is given by

$$\begin{aligned}&\left(\gamma_j-1\right)T_{j-1}^{t+1}+\left(\frac{\zeta_j}{\Delta t}+2+\delta_j\beta_j^{t+1}\right)T_j^{t+1}-\left(\gamma_j+1\right)T_{j+1}^{t+1}-\delta_j\beta_j^{t+1}T_{bl,a}^{t+1}=\\&=\left(1-\gamma_j\right)T_{j-1}^{t}+\left(\frac{\zeta_j}{\Delta t}-2-\delta_j\beta_j^{t}\right)T_j^{t}+\left(\gamma_j+1\right)T_{j+1}^{t}+\delta_j\beta_j^{t}T_{bl,a}^{t}+\delta_j\left(q_{m,j}^{t+1}+q_{m,j}^{t}\right)\end{aligned}\quad , \tag{4.8}$$

where $\zeta_j=\rho_j c_j\frac{\Delta r_{j-1}^2+\Delta r_j^2}{k_j}$, $\delta_j=\frac{\Delta r_{j-1}^2+\Delta r_j^2}{2k_j}$ and $\gamma_j=\frac{\omega}{2r_j}\frac{\Delta r_{j-1}^2+\Delta r_j^2}{\Delta r_{j-1}+\Delta r_j}$, with ω equal to 1 for polar coordinates and equal to 2 for spherical coordinates. For $\Delta r_{j-1}=\Delta r_j=$constant, this equation is further simplified.

The Pennes bioheat equation (4.8) is applied for every not fictitious *j*-node while the corresponding nodes *j*-1, *j*+1 may be regular or fictitious nodes in the same tissue layer. It is important to mention, here, that it is applied for both spherical and cylindrical elements with the difference that ω is equal to 1 for polar and 2 for spherical coordinates The nodes, regular and fictitious, are described in Section 4.2.

4.2 Interface boundary condition

The formulation of the interface boundary condition is made by inserting to the model fictitious nodes. In general, there is no node on the interface. Instead there are regular nodes before and one after the interface. To be more specific, a schematic of the regular and fictitious nodes at the interface can be shown in Figure 4.1. The regular nodes are full (black) and the fictitious are empty inside (white). The *j*-node is the last regular node of the left tissue layer (for now call it *j*-layer) and the (*j*+1)-node is the first regular node of the (*j*+1)-layer. An imaginary node $\left(j+1\right)''$ with the properties of the *j*-layer and an imaginary node j'' with the (*j*+1)-layer

properties are assumed. Note that Δr_{j-1}, denoting the distance between the node *j*-1 and *j*, is equal to the distance between *j* and $(j+1)''$, Δr_j and, similarly, the distance between j'' and *j*+1, $\Delta r_{j''}$, is equal with the distance between *j*+1 and *j*+2, Δr_{j+1}, but mostly $\Delta r_j \neq \Delta r_{j''}$. The boundary interface condition is formulated by equating the heat flow rate from the node *j* to $(j+1)''$ with the heat rate from j'' to (*j*+1).

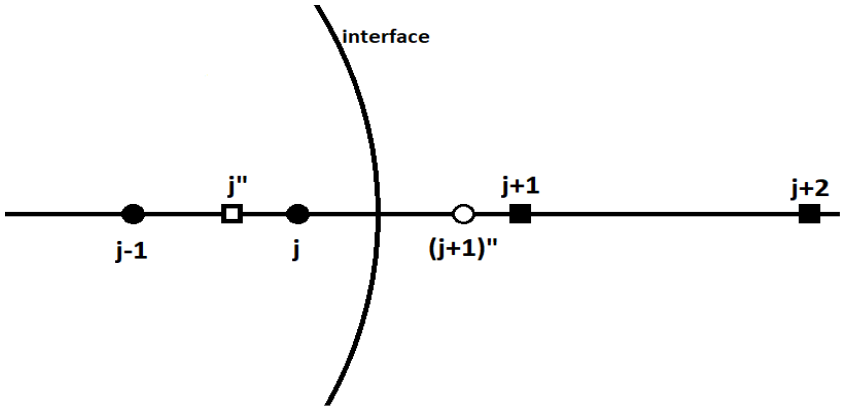

Figure 4.1 : Interface schematic of regular and fictitious nodes

4.2.1 Cylindrical coordinates

For cylindrical coordinates, the heat flow rate between two points $\dot{Q}_{1\to 2}\,(W)$ (as presented in Appendix A) is calculated by

$$\dot{Q}_{1\to 2} = -k\,A(r)\frac{dT}{dr} = -\varphi\, h\, k\frac{(T_2 - T_1)}{\ln\left(\frac{r_2}{r_1}\right)} \quad , \tag{4.9}$$

where φ (rad) the angle of the sector and h the height of the cylinder and $k\ (W/(m\,K))$ the layer thermal conductivity of the layer between r_1, r_2. Applying (4.9) for $j \to (j+1)''$ and $j'' \to (j+1)$ and equating it is deduced that

$$k_j \frac{\left(T_{(j+1)''} - T_j\right)}{\ln\left(\frac{r_{(j+1)''}}{r_j}\right)} = k_{j+1} \frac{\left(T_{j+1} - T_{j''}\right)}{\ln\left(\frac{r_{j+1}}{r_{j''}}\right)} \ , \tag{4.10}$$

where ($-\varphi_s h$) was eliminated. As two additional unknowns have been inserted (two imaginary nodes), one more equation is needed. This is taken by the fact that the temperature on the interface T_{ifc} has to be common. It is proven in Appendix A that in a cylindrical shell the temperature at radius r, when $r_1 < r < r_2$, can be calculated by

$$T(r) = T_r = \frac{T_{r_1} \ln\left(\frac{r}{r_2}\right) - T_{r_2} \ln\left(\frac{r}{r_1}\right)}{\ln\left(\frac{r_1}{r_2}\right)} \tag{4.11}$$

Applying Eq. (4.11) for $j \to (j+1)''$ and $j'' \to (j+1)$ for the common point of interface, and equating results to

$$\frac{T_j \ln\left(\frac{r_{ifc}}{r_{(j+1)''}}\right) - T_{(j+1)''} \ln\left(\frac{r_{ifc}}{r_j}\right)}{\ln\left(\frac{r_j}{r_{(j+1)''}}\right)} = T_{ifc} = \frac{T_{j''} \ln\left(\frac{r_{ifc}}{r_{j+1}}\right) - T_{j+1} \ln\left(\frac{r_{ifc}}{r_{j''}}\right)}{\ln\left(\frac{r_{j''}}{r_{j+1}}\right)} \tag{4.12}$$

Thus, Eq. (4.10) and Eq. (4.12) are applied for the imaginary nodes $(j+1)''$ and j'' respectively.

4.2.2 Spherical coordinates

Similar work is done in the spherical elements. The heat flow rate between two points $\dot{Q}_{1\to 2}(W)$ for a spherical shell with thermal conductivity of k and spherical shell surface area $A(r)=2\varphi r^2$ is proven in Appendix A to be calculated by

$$\dot{Q}_{1\to 2}=-k\cdot A(r)\cdot\frac{dT}{dr}=-2\varphi k\frac{T_1-T_2}{\frac{1}{r_2}-\frac{1}{r_1}}\ , \tag{4.13}$$

where φ (*rad*) the angle of the sector. By equating the heat rates between points $j\to(j+1)''$ and $j''\to(j+1)$ it is found that

$$-2\varphi_s k_j\frac{T_j-T_{(j+1)''}}{\frac{1}{r_{(j+1)''}}-\frac{1}{r_j}}=-2\varphi_s k_{j+1}\frac{T_{j''}-T_{j+1}}{\frac{1}{r_{j+1}}-\frac{1}{r_{j''}}}\ . \tag{4.14}$$

Of course, ($-2\varphi_s$) is eliminated. The second equation is obtained from the common interface temperature (T_{ifc} (in ^oC)). The temperature at radius r in a cylindrical shell, where $r_1<r<r_2$ is proven in Appendix A to be calculated by

$$T(r)=T_r=\frac{r_2T_{r_2}-r_1T_{r_1}}{r_2-r_1}+\frac{T_{r_1}-T_{r_2}}{\frac{r}{r_1}-\frac{r}{r_2}}\ . \tag{4.15}$$

Applying (4.15) for points $j\to(j+1)''$ and $j''\to(j+1)$ for the common point of interface, results to

$$\frac{r_{(j+1)''}T_{(j+1)''}-r_jT_j}{r_{(j+1)''}-r_j}+\frac{T_j-T_{(j+1)''}}{\frac{r_{ifc}}{r_j}-\frac{r_{ifc}}{r_{(j+1)''}}}=T_{ifc}=\frac{r_{j+1}T_{j+1}-r_{j''}T_{j''}}{r_{j+1}-r_{j''}}+\frac{T_{j''}-T_{j+1}}{\frac{r_{ifc}}{r_{j''}}-\frac{r_{ifc}}{r_{j+1}}}\ . \tag{4.16}$$

Then, Eq. (4.14) and Eq. (4.16) are applied for the imaginary nodes $(j+1)''$ and j'' respectively.

4.3 Core boundary condition

The heat fluxes $q_{ifc,s}$ result from Eq. (4.9) and (4.13) for cylindrical and spherical coordinates respectively as [11]

$$q_{ifc} = k_j \frac{T_j - T_{j+1}}{r_{ifc} \ln\left(\frac{r_j}{r_{j+1}}\right)} \tag{4.17}$$

and

$$q_{ifc} = k_j \frac{T_j - T_{j+1}}{\frac{r_{ifc}^2}{r_j} - \frac{r_{ifc}^2}{r_{j+1}}} \ , \tag{4.18}$$

where for the core node j=1. For the core boundary condition, Eq. (3.36) is used.

After, discretizing the core boundary equation and using the Crank Nicholson method the discretized equation at the core node reads as

$$\begin{aligned} &\left(\frac{\zeta_c}{\Delta t} + \delta_c \beta_j^{t+1} + \sum_{s=1}^{S}(\varphi_s)\right) T_j^{t+1} - \sum_{s=1}^{S}\left(\varphi_s T_{jnext,s}\right) - \delta_c \beta_j^{t+1} T_{bl,a}^{t+1} = \\ &= \left(\frac{\zeta_c}{\Delta t} - \delta_c \beta_j^{t} - \sum_{s=1}^{S}(\varphi_s)\right) T_j^{t} + \sum_{s=1}^{S}\left(\varphi_s T_{jnext,s}\right) + \delta_c \beta_j^{t} T_{bl,a}^{t} + \delta_c \left(q_{m,j}^{t+1} + q_{m,j}^{t}\right) \end{aligned} \ , \tag{4.19}$$

where in cylinders $\begin{cases} \zeta_c = \dfrac{2\pi r_j^2 \ln\left(\dfrac{r_{jnext,s=1}}{r_j}\right)}{k_j}\rho_j c_j \\ \delta_c = \dfrac{\pi r_j^2 \ln\left(\dfrac{r_{jnext,s=1}}{r_j}\right)}{k_j} \end{cases}$

and in the sphere (head) $\begin{cases} \zeta_c = \dfrac{4\pi r_j^3\left(\dfrac{1}{r_j}-\dfrac{1}{r_{jnext,s=1}}\right)}{3k_j}\rho_j c_j \\ \delta_c = \dfrac{2\pi r_j^3\left(\dfrac{1}{r_j}-\dfrac{1}{r_{jnext,s=1}}\right)}{3k_j} \end{cases}$.

The subscript "*c*" denotes the core, while $r_{jnext,s=1}$ is picked for *s*=1 which does not affect the solution since $r_{jnext,s=1} = r_{jnext,s=2} = ... = r_{jnext,s=S}$. It would be useful, also, to note that the node $jnext,s$ can be the imaginary node if the core layer has only one node. The only element in which the core contains more than one node is the head element (Table 2.3).

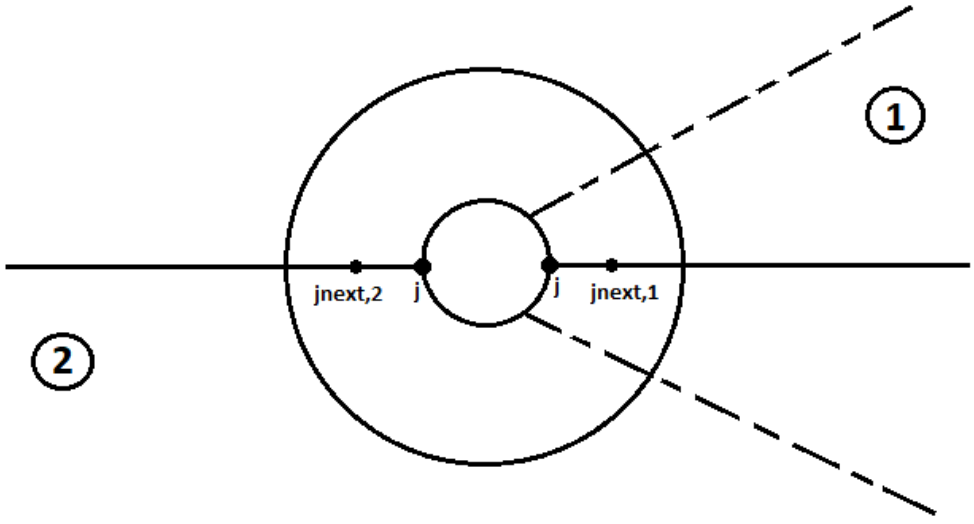

Figure 4.2 : Representation of the core boundary condition nodes

4.4 Skin boundary condition

It is assumed that the heat loss from the skin $q_{sk}\ \left(W/m^2\right)$ equals the heat flux due to conduction $q_j\ \left(W/m^2\right)$ reaching from the sector last regular node *j* to the skin and for cylindrical elements can be calculated by

$$q_j = k_j \frac{T_j - T_{sk}}{r_{sk} \ln\left(\frac{r_{sk}}{r_j}\right)} = q_{sk} \tag{4.20}$$

with *j* being the sector last regular node k_j the thermal conductivity of *j* node and T_{sk} the skin temperature at radius r_{sk} such that $r_{sk} = r_j + \Delta r_j/2$. The temperature T_{sk} can be calculated for cylindrical layer-shells by using Eq. (4.11) resulting in

$$T_{sk} = \frac{T_j \ln\left(\frac{r_{sk}}{r_{(j+1)''}}\right) - T_{(j+1)''} \ln\left(\frac{r_{sk}}{r_j}\right)}{\ln\left(\frac{r_j}{r_{(j+1)''}}\right)}\ , \tag{4.21}$$

with *j* being the sector last regular node and *j*+1 the next (imaginary) node. By combining the equations (3.37), (3.38), (4.20), (4.21) the discretized boundary conditions for cylindrical elements is

$$\left[\frac{k_j}{r_{sk}\ln\left(\frac{r_{sk}}{r_j}\right)}\left(1-\frac{\ln\left(\frac{r_{sk}}{r_{(j+1)''}}\right)}{\ln\left(\frac{r_j}{r_{(j+1)''}}\right)}\right)-\frac{\ln\left(\frac{r_{sk}}{r_{(j+1)''}}\right)}{\ln\left(\frac{r_j}{r_{(j+1)''}}\right)R_{lT}}\right]T_j+\left(\frac{\ln\left(\frac{r_{sk}}{r_j}\right)}{\ln\left(\frac{r_j}{r_{(j+1)''}}\right)R_{lT}}+\frac{k_j}{r_{sk}\ln\left(\frac{r_j}{r_{(j+1)''}}\right)}\right)T_{(j+1)''}\ , \tag{4.22}$$

$$= \frac{p_{sk} - p_{air}}{R_{e,lT}} - \frac{T_o}{R_{lT}}$$

where R_{lT} and $R_{e,lT}$ are described in Subsection 3.3.5, p_{air} is described in Subsection 3.3.3 and T_o in Subsection 3.4.3.

For the spherical element, similarly, the heat flux due to conduction from the sector last

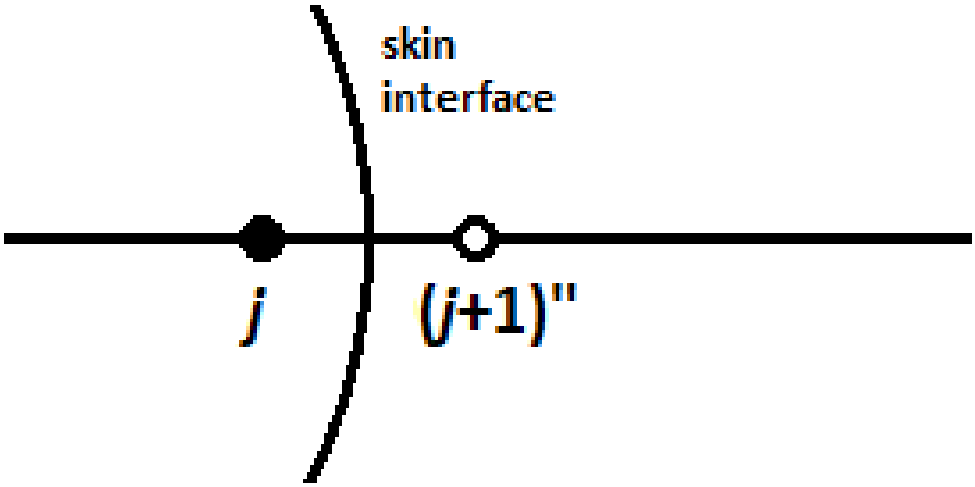

Figure 4.3 : Representation of the skin boundary conditions nodes

regular node *j* to the skin is

$$q_j = k_j \frac{T_j - T_{sk}}{r_{sk}^2 \left(\frac{1}{r_j} - \frac{1}{r_{sk}} \right)} = q_{sk} \ , \tag{4.23}$$

with T_{sk} the skin temperature at radius r_{sk} such that $r_{sk} = r_j + \Delta r_j / 2$. The temperature T_{sk} as function of T_j and $T_{(j+1)"}$ for a spherical shell (using Eq. (4.15)) can be calculated by

$$T_{sk} = \frac{r_{(j+1)"} T_{(j+1)"} - r_j T_j}{r_{(j+1)"} - r_j} + \frac{T_j - T_{(j+1)"}}{\frac{r_{sk}}{r_j} - \frac{r_{sk}}{r_{(j+1)"}}} \ . \tag{4.24}$$

Finally, by using equations (3.37), (3.38), (4.23), (4.24) and the fact that $r_{sk} = r_j + \Delta r_j / 2$, the discretized core boundary condition for spherical coordinates can be calculated by

$$\left[\frac{k_j}{r_{sk}^2\left(\frac{1}{r_j}-\frac{1}{r_{sk}}\right)}\left(1-\frac{r_j}{2r_{sk}}\right)-\frac{r_j}{2r_{sk}R_{lT}}\right]T_j \;-\; \left[\frac{r_{(j+1)''}}{2r_{sk}}\left(\frac{k_j}{r_{sk}^2\left(\frac{1}{r_j}-\frac{1}{r_{sk}}\right)}+\frac{1}{R_{lT}}\right)\right]T_{(j+1)''} \quad . \quad (4.25)$$

$$= \frac{p_{sk}-p_{air}}{R_{e,lT}}-\frac{T_o}{R_{lT}}$$

4.5 Blood arterial and blood pool temperature analysis

The blood arterial temperature of each element given by Eq. (3.14) is analyzed and calculated by the approximation

$$\mathrm{T}_{bl,a}=\frac{T_{bl,p}\sum_{j=1}^{J}\beta_j V_j}{h_x+\sum_{j=1}^{J}\beta_j V_j}+\frac{h_x\sum_{j=1}^{J}\beta_j V_j T_j}{\sum_{j=1}^{J}\beta_j V_j\left(h_x+\sum_{j=1}^{J}\beta_j V_j\right)}\,, \quad (4.26)$$

where J is the element number of nodes. The blood pool temperature $T_{bl,p}$ (^oC) having a unique value and is a function of all the node temperatures indicating the contribution of the circulatory system to the human heat transfer. It is calculated by [11]

$$T_{bl,p}=\frac{\sum_{e}^{E}\left(\frac{\sum_{j}^{J,e}\beta_{e,j}V_{e,j}}{h_{x,e}+\sum_{j}^{J,e}\beta_{e,j}V_{e,j}}\cdot\sum_{j}^{J,e}\beta_{e,j}V_{e,j}T_{e,j}\right)}{\sum_{e}^{E}\left(\frac{\left(\sum_{j}^{J,e}\beta_{e,j}V_{e,j}\right)^2}{h_{x,e}+\sum_{j}^{J,e}\beta_{e,j}V_{e,j}}\right)}\,, \quad (4.27)$$

where J,e is the number of nodes of the e-element and E is the number of elements. The equation can be rewritten as

$$\sum_{e}^{E}\left(\frac{\sum_{j}^{J,e}\beta_{e,j}V_{e,j}}{h_{x,e}+\sum_{j}^{J,e}\beta_{e,j}V_{e,j}}\cdot\sum_{j}^{J,e}\beta_{e,j}V_{e,j}T_{e,j}\right)-\sum_{e}^{E}\left(\frac{\left(\sum_{j}^{J,e}\beta_{e,j}V_{e,j}\right)^{2}}{h_{x,e}+\sum_{j}^{J,e}\beta_{e,j}V_{e,j}}\right)T_{bl,p}=0\ . \qquad (4.28)$$

The temperature $T_{bl,a}$ is used in the calculation of both the bioheat equation and the core boundary condition. Thus it is necessary to be appropriately discretized. The temperature $T_{bl,p}$, as a unique value for the whole body, is imported as an additional unknown temperature and for this current work $T_{bl,p}=T_{j=N+1}$. By substituting the Eq. (4.26) into the bioheat equation, the coefficients of the unknown temperatures are accordingly modified and one more unknown is added. Thus, for every *i*-node that the bioheat equation is applied, the coefficients bl_{ij} of the $\text{Blood}_{\text{mat}}$ will be formed as

$$bl_{ij}=\delta_{cr,ij}\,\delta_i\beta_j+\delta_i\beta_i\beta_jV_jB'_{x,e} \qquad (4.29)$$

for every *j* regular node,

$$bl_{ij}=0 \qquad (4.30)$$

for every *j* imaginary node and

$$bl_{ij}=\frac{\sum_{n}^{N,e}\beta_nV_n}{h_{x,e}+\sum_{n}^{N,e}\beta_nV_n}\delta_i\beta_i \qquad (4.31)$$

for $j=N+1$, where

$$B'_{x,e}=-\frac{h_{x,e}}{\sum_{n}^{N,e}\beta_nV_n\left(h_{x,e}+\sum_{n}^{N,e}\beta_nV_n\right)}\ ,$$

where *N,e* is the number of nodes of the *e*-element and $\delta_{cr,ij}$ is the Kronecker delta and is equal to 1 when $i = j$ and equal to 0 when $i \neq j$. Similar work is done in the core boundary equation.

The system of linear equations is completed with the equation for $T_{bl,p}$ which includes all the nodes of all body elements. Eq. (4.28), is accordingly modified and the coefficients bl_{ij} of the $\text{Blood}_{\text{mat}}$ for $i = N+1$ are given by

$$bl_{i=N+1,j} = \begin{Bmatrix} \dfrac{\sum_{n}^{N,e} \beta_n V_n}{h_{x,e} + \sum_{n}^{N,e} \beta_n V_n} \beta_j V_j, & for\ j = 1,2,\ldots,N \\ \sum_{e}^{E} \left(\dfrac{\left(\sum_{n}^{N,e} \beta_{e,n} V_{e,n} \right)^2}{h_{x,e} + \sum_{n}^{N,e} \beta_{e,n} V_{e,n}} \right), & for\ j = N+1 \end{Bmatrix} \tag{4.32}$$

and $B_{mat,\, i=N+1} = 0$.

4.6 The mesh and equation application

The FDM mesh along with the applied equation are presented in detail. The nodes can be either regular or imaginary. The imaginary nodes are useful in the solving procedure and are not concerned as actual body temperatures. Although they can be omitted by combining some equations, in the present work they are preserved. The mesh presentation will be through an example of a particular element used, although the same strategy is followed for all elements.

In Figure 4.4, a schematic of the neck element is presented. It is important to note that the actual size of the tissues is not kept in order to have better clarity. For instance the fat and skin tissues are much narrower. However, the node sequence is preserved. Every layer has different

color and the dashed line separates the element into two sectors of 180^o : the anterior and posterior sectors. For every sector a 1D mesh is shown, where the full (black inside) points are regular nodes and the empty (white inside) points indicate imaginary nodes.

Within a layer, if the layer has a width of W (in m) and there is a number of regular nodes N (Table 2.3) the distance between the nodes of this layer dr (m) is fixed and calculated by $dr = W / N$. All the nodes (regular and fictitious) are equally spaced, while the first regular node is at distance $dr / 2$ from the interface of between the current and previous layer (if existed). For the core layer the node is considered to be on the interface of the core and next layer.

For every interface, except for the last skin surface, there are two imaginary nodes; one for the "left" layer with its properties put into the "right" layer and one with properties of the "right" layer put into the left. For the skin surface there is one imaginary node considered to be at distance $dr / 2$ outside the skin surface.

The first node of every element is the core node. Then, if there are more regular nodes are numbered consecutively. For every interface between layers the imaginary node of the previous layer is numbered first and then the imaginary node of the following layer is numbered. The imaginary node of the last layer is the last for the sector. The numerating is continued to the next sector from the first node after the core node (the core node is common for every sector of the element). Note that there must be some symmetry between the meshes of each sector.

4.7 The linear algebraic system

For the human heat transfer problem to be solved with FDM, a linear system of equations is going to be solved as

$$\left[A_{mat}\right]_{(N+1)\times(N+1)} \left\lfloor T \right\rfloor_{(N+1)\times 1} = \left\lfloor B_{mat} \right\rfloor_{(N+1)\times 1} \ .$$

where N is the number of all the nodes of the problem and the (N+1) equation refers to the additional unknown temperature $T_{bl,p}$ which is regarded as unknown. The T vector includes all the N node temperatures plus the $T_{bl,p}$ temperature. The matrix A_{mat} includes the coefficients of the unknowns for each linear equation and the vector B_{mat} the known right hand side. The matrix A_{mat} is the summation of $Blood_{mat}$ and $Conduction_{mat}$. The $Conduction_{mat}$ is calculated once and is going to include all the coefficients constant with time and thus not changing with iterations. The $Blood_{mat}$ includes all the temperature coefficients that change with time; such coefficients are influenced by the energy equivalent β, the heat transfer coefficients h_c, h_R and thus $R_{e,lT}$, R_{lT}, etc. and therefore it is changing with time.

The formulation of linear system of equations for the FDM is presented. For each regular node except for the core node (for this example $j = 4,5,6,7,10,11,14,15,16,17,21,22,23,24,27,28,31,32,33,34$) the Pennes bioheat equation (4.8) is applied in which the previous and following node temperature (might be imaginary node of the current layer) are included. For the two imaginary nodes $(j = 2,3,8,9,12,13,19,20,25,26,29,30)$ before and after each interface two equations are needed. For a cylinder, equations (4.10) and (4.12) are applied, while for a sphere, equations (4.14) and (4.16) are used. For the core node ($j = 1$) the core boundary condition, Eq. (4.19), is applied just once for each element with careful selection over the constants used for cylinders or the sphere. Note, that this equation involves all nodes that following the core node for every sector. For the last imaginary node of every sector skin layer $(j = 8,35)$, in the cylinder case, Eq. (4.22) is applied, while in the sphere, Eq. (4.25) is selected. Finally, the linear system is completed with the Eq. (4.28) referring to $T_{bl,p}$.

It is noted that in Figure 4.4 the distance between nodes 6 and 7 is the same with the distance between nodes 7 and 8. Node 8 is drawn next to node18 because the specific distance between these nodes is much larger than the distances between the nodes of the next tissues, the width of which is much smaller than the width of the second tissue.

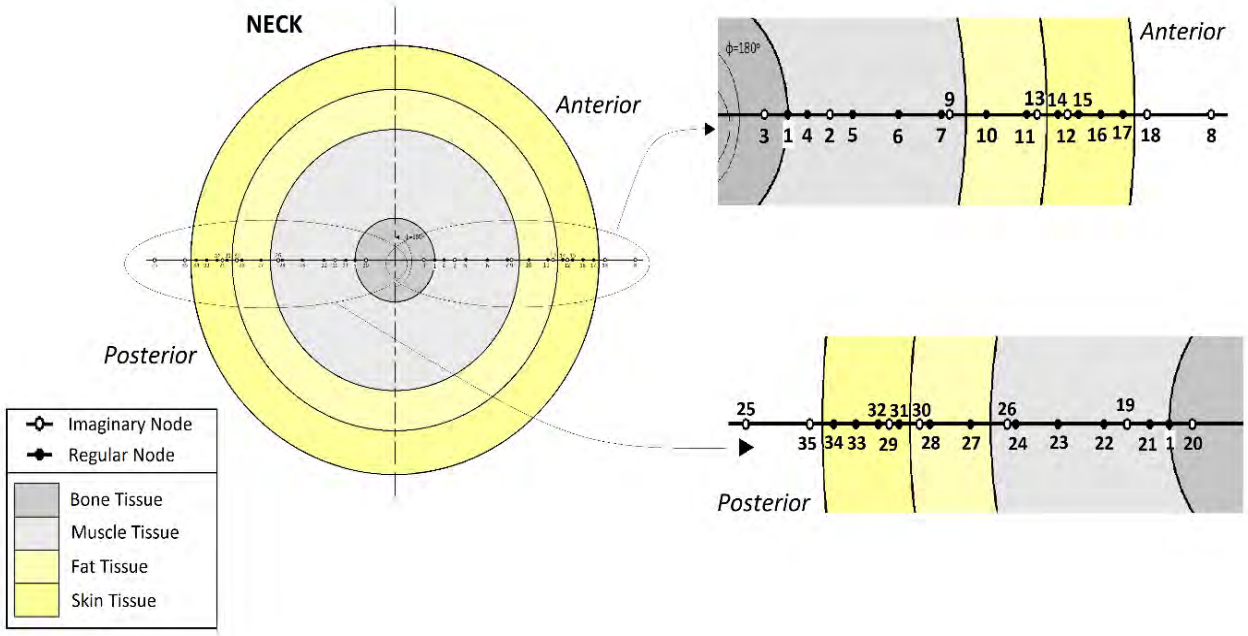

Figure 4.4 : Schematic view of the neck element.

5 Model verification and results

Following the analysis of the Fiala Model some benchmark problems are solved to validate the correctness and accuracy of the developed code. They include two single-layer and two multi-layer problems for specific body elements.

5.1 Single-layer elements

Two single-layer elements are considered. One is cylindrical and the other one is spherical. It is assumed that they consist of one uniform layer (tissue).

5.1.1 Single-layer cylindrical element test

The first test is conducted in one cylindrical element, representing a leg element. The cylinder's inner core is at radius of 2.2 cm, the outer (skin) radius at 5.48 cm and the tissue between is a homogenous muscle tissue. The muscle tissue has the following properties:

- Density $\rho = 1085\ kg/m^3$,
- thermal conductivity $k = 0.42\ W/(m\,K)$
- heat capacity $c = 3768\ J/(kg\,K)$
- blood perfusion rate of $w_{bl} = 0.001\ s^{-1}$

The initial cylinder temperature is $T = 0^o C$ and no blood flows into the element. The surrounding air temperature and mean radiant temperature are at $T_{air} = T_{mrt} = 0^o C$. At time t=0 s, blood starts to flow with a steady and given temperature of $T_{bl,a} = 37^o C$ enabling heat flow

from the core, while extra metabolic heat is produced in the muscle tissue of $q_m = 600\ W/m^3$. As a result, the temperature of the cylinder rises and converges in a steady state value. The temperature inside the muscle tissue is not uniform. It is significant to mention that in [11] a comparison is presented with the analytic solution of the bioheat equation introduced by Eberhart. In this test the convective and radiation heat transfer coefficient are taken as $h_c = 5\ W/\left(m^2\ K\right)$ and $h_r = 0$. Finally, the irradiation and sweat evaporation are switched off.

This test is simulated with 35 nodes, as shown in Figure 5.1. The first core node is at radius $r_1 = 0.022\ m$ with the rest of the nodes equally spaced with $\Delta r \approx 0.09791\ cm$ so that the skin radius (at $r_{sk} = 0.0548\ m$) is in the middle of the 34th and 35th node radius.

For the first core node the core boundary condition (4.19) for cylinders is applied with $j \to 1,\ jnext,1 \to 2$ as

$$\left(\frac{\zeta_c}{\Delta t} + \delta_c \beta_1^{t+1} + \varphi_1\right) T_1^{t+1} - \varphi_1 T_2 - \delta_c \beta_1^{t+1} T_{bl,a}^{t+1} = \left(\frac{\zeta_c}{\Delta t} - \delta_c \beta_1^{t} - \varphi_1\right) T_1^{t} + \varphi_1 T_2 + \delta_c \beta_1^{t} T_{bl,a}^{t} + \delta_c \left(q_{m,1}^{t+1} + q_{m,1}^{t}\right)$$

with

$$\zeta_c = \frac{2\pi r_1^2 \ln\left(r_2/r_1\right)}{k_1} \rho_1 c_1,\ \delta_c = \frac{\pi r_1^2 \ln\left(r_2/r_1\right)}{k_1},\ \varphi_1 = 2\pi,\ \beta_1^t = \rho_{bl}\, c_{bl}\, w_{bl,1}^t,\ T_{bl,a}^{t+1} = T_{bl,a}^t = 37\ ^oC\ \ \forall t\ .$$

For the last (35th) and imaginary node the skin boundary condition Eq. (4.22) for $j \to 34$ *and* $\left(j+1\right)'' \to 35$ as

$$\left[\frac{k_{34}}{r_{sk} \ln\left(\frac{r_{sk}}{r_{34}}\right)}\left(1 - \frac{\ln\left(\frac{r_{sk}}{r_{35}}\right)}{\ln\left(\frac{r_{34}}{r_{35}}\right)}\right) - \frac{\ln\left(\frac{r_{sk}}{r_{35}}\right)}{\ln\left(\frac{r_{34\,j}}{r_{35}}\right) R_{lT}}\right] T_{34} + \left(\frac{\ln\left(\frac{r_{sk}}{r_{34}}\right)}{\ln\left(\frac{r_{34}}{r_{35}}\right) R_{lT}} + \frac{k_{34}}{r_{sk} \ln\left(\frac{r_{34}}{r_{35}}\right)}\right) T_{35} = \frac{p_{sk} - p_{air}}{R_{e,lT}} - \frac{T_o}{R_{lT}}$$

where $R_{lT} = 1/h$, $R_{e,lT} = 1/(L_a\, h_c)$, $p_{air} = RH\; p_{air,sat}$, $p_{sk} = \dfrac{\dfrac{p_{air}}{R_{e,lT}} + \lambda_{H^2O}\dfrac{1}{A_{sk}}\dfrac{dm_{sw}}{dt} + \dfrac{p_{s,sk}}{R_{e,sk}}}{\dfrac{1}{R_{e,lT}} + \dfrac{1}{R_{e,sk}}}$,

$\dfrac{dm_{sw}}{dt} = 0$ and $T_o = 0\,^oC$ because the irradiation is switched off and $T_{air} = T_{mrt} = 0^oC$.

For every other node between – assume *j* – the bioheat equation (4.8) is applied for polar coordinates and given by

$$\begin{aligned}&\left(\gamma_j - 1\right)T_{j-1}^{t+1} + \left(\frac{\zeta_j}{\Delta t} + 2 + \delta_j\beta_j^{t+1}\right)T_j^{t+1} - \left(\gamma_j + 1\right)T_{j+1}^{t+1} - \delta_j\beta_j^{t+1}T_{bl,a}^{t+1} = \\ &= \left(1-\gamma_j\right)T_{j-1}^{t} + \left(\frac{\zeta_j}{\Delta t} - 2 - \delta_j\beta_j^{t}\right)T_j^{t} + \left(\gamma_j + 1\right)T_{j+1}^{t} + \delta_j\beta_j^{t}T_{bl,a}^{t} + \delta_j\left(q_{m,j}^{t+1} + q_{m,j}^{t}\right)\end{aligned},$$

for $j = 2,3,\ldots,34$, where $\zeta_j = \rho_j c_j \dfrac{\Delta r_{j-1}^2 + \Delta r_j^2}{k_j}$, $\delta_j = \dfrac{\Delta r_{j-1}^2 + \Delta r_j^2}{2k_j}$, $\gamma_j = \dfrac{\omega}{2r_j}\dfrac{\Delta r_{j-1}^2 + \Delta r_j^2}{\Delta r_{j-1} + \Delta r_j}$,

$\beta_j^t = \rho_{bl}\, c_{bl}\, w_{bl,j}^t$ and $q_{m,j}^t = 600\; W/m^3$, $\forall t$.

The temperatures shown in Table 5.1 are for steady state conditions and from three nodes, the inner core temperature at r_1, the outer skin temperature at r_{sk} and a node between at $r_{btw} = 0.0493\; m$. The results are, then, compared with the results of Fiala [11]. Note that the node at $r_{btw} = 0.0493\; m$ is selected for comparison reasons and it is not a mesh node. Its temperature is computed via Eq. (4.11) using the nearest node temperatures i.e. nodes 28 and 29 and is given by

$$T_{r_{btw}} = \frac{r_{29}T_{r_{29}} - r_{28}T_{r_{28}}}{r_{29} - r_{28}} + \frac{T_{r_{28}} - T_{r_{29}}}{\dfrac{r_{btw}}{r_{28}} - \dfrac{r_{btw}}{r_{29}}}.$$

An important feature of Fiala Model is that it predicts the transient behavior of temperatures of the human body i.e. the temperature rate of change before coming to a steady state. Consequently, it is crucial to verify that the transient problem also works fine. Table 5.2, Table 5.3 and Table 5.4 show the results for core, skin and the node between respectively of both the Fiala Model and the present work for comparison reasons. Very good agreement is obtained.

To better visualize the temperature changes through time, Figure 5.2 presents the comparison between a) the temperature results of the present work with the analytic solution of the Eberhart bioheat equation and b) the Fiala results with the same analytic solution [11]. Also, the steady state temperature distribution is presented in Figure 5.3 in which only the temperatures of the regular node plus the skin temperature are considered.

With this test conducted we have been able to verify

- the convergence of the finite difference method
- the accuracy of the core boundary condition in cylindrical coordinates (for cylinders)
- the accuracy of the outer skin boundary condition in cylindrical coordinates (for cylinders)
- the heat transfer within a homogeneous tissue in cylindrical coordinates (for cylinders)
- the transient temperature results for the equations discretized in cylindrical coordinates

Radius [cm]	**2.2**	**4.93**	**5.48**
Fiala Model [^oC]	36.85	34.0	32.65
Present Work [^oC]	36.87	34.3	32.58

Table 5.1 : Comparison of steady state values for the single-layer cylindrical element test with corresponding results in [6]

Time [min]	**10**	**20**	**30**	**40**	**50**	**60**	**70**	**80**	**90**	**100**
Fiala Model [^oC]	16.3	25.38	30.46	33.3	34.88	35.74	36.24	36.48	36.62	36.73
Present Work [^oC]	15.9	25.11	30.32	33.23	34.86	35.76	36.26	36.53	36.68	36.77

Table 5.2 : Comparison of cylinder core temperature for single-layer cylindrical element test with corresponding results in [6]

Time [min]	**10**	**20**	**30**	**40**	**50**	**60**	**70**	**80**	**90**	**100**
Fiala Model [^oC]	15.25	23.23	27.52	29.86	31.08	31.8	32.17	32.42	32.48	32.59
Present Work [^oC]	14.64	22.9	27.33	29.72	31.02	31.73	32.12	32.33	32.44	32.51

Table 5.3 : Comparison of outer skin temperature for single-layer cylindrical element test with corresponding results in [6]

Time [*min*]	**10**	**20**	**30**	**40**	**50**	**60**	**70**	**80**	**90**	**100**
Fiala Model [^oC]	15.87	24.27	28.79	31.28	32.61	33.37	33.74	33.96	34.09	34.18
Present Work [^oC]	15.25	23.99	28.69	31.25	32.63	33.39	33.8	34.03	34.15	34.22

Table 5.4: Comparison of temperature of a node inside the cylinder (r=4.93cm) for single-layer cylindrical element test with corresponding results in [6]

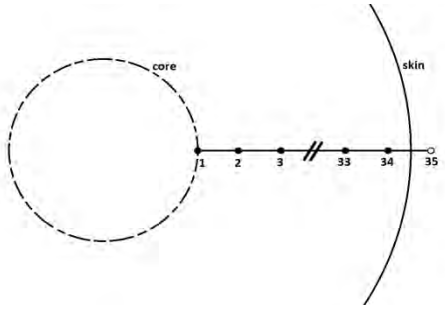

Figure 5.2 : Schematic of the homogeneous cylinder mesh

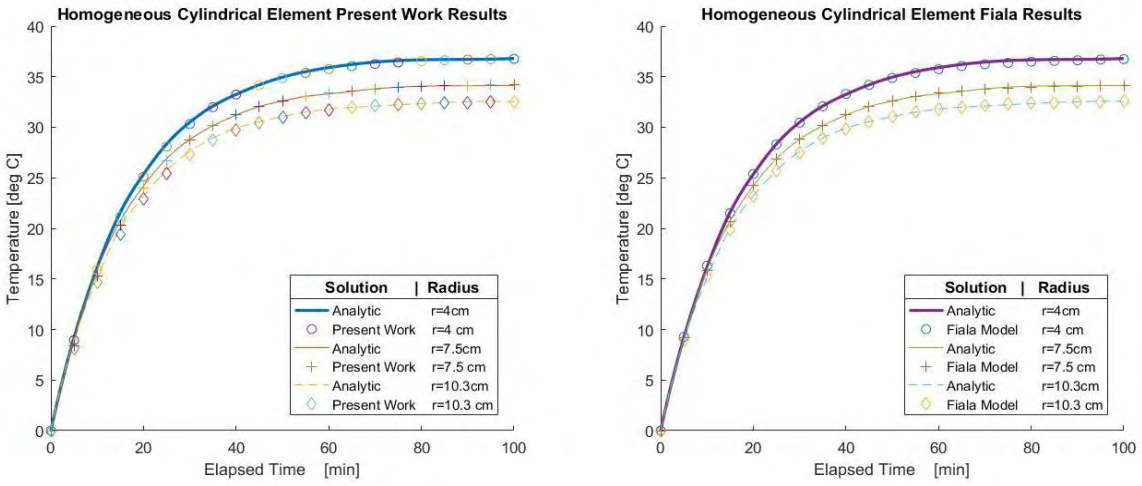

(a) (b)

Figure 5.1 : Comparison of the analytical results for a cylindrical element in [11] with (a) the present results and (b) the Fiala result

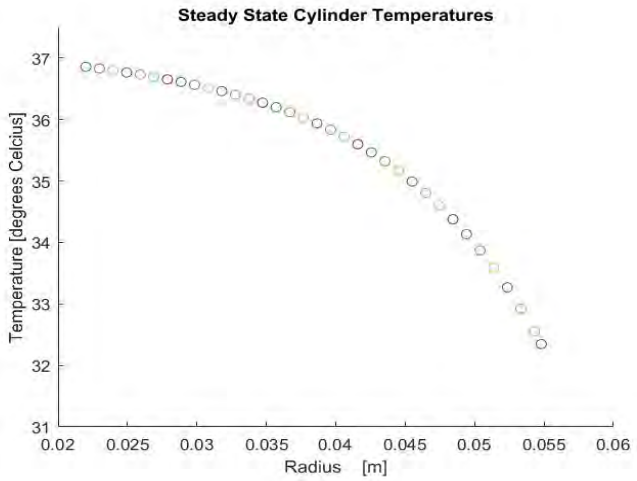

Figure 5.3 : Steady state temperature distribution in the annular cylinder

5.1.2 Single-layer spherical element test

The second test is conducted in one spherical element to verify the equations of heat transfer equation and boundary conditions in spherical coordinates. In this test, a spherical element is made up of brain tissue with an outer radius of 10.3 cm and an inner core radius of 4 cm. The tissue inside the sphere is uniform and has the following properties:

- density $\rho = 1080\ kg/m^3$,
- thermal conductivity $k = 0.49\ W/(m\,K)$
- heat capacity $c = 3850\ J/(kg\,K)$

The metabolic heat production and blood perfusion rate are equal to zero ($q_m = w_{bl} = 0$). Thus the arterial blood temperature does not influence the solution whatsoever. Initially, the sphere is in a homogeneous temperature $T_{initial} = 37\ ^oC$. The temperature of the surrounding environment is at 0 ^oC which means that because there is neither heat production nor blood perfusion the sphere temperature is expected to constantly being decreased till it reaches zero degrees Celsius. The (overall) surface heat transfer coefficient is imposed to $h = 20\ W/(m^2\,K)$, while the irradiation and sweat evaporation are switched off.

For the single-layer spherical element test 15 nodes were used. The first core node is at radius $r_1 = 0.04\,m$ and the rest of the nodes were equally spaced with $\Delta r \simeq 0.4666\,cm$ so that the skin $(r_{sk} = 0.104\,m)$ is in the middle of 14th and 15th node.

For the first core node the core boundary condition (4.19) for spherical coordinates is applied with $j \to 1,\ jnext, 1 \to 2$ as

$$\left(\frac{\zeta_c}{\Delta t}+\delta_c\beta_1^{t+1}+\varphi_1\right)T_1^{t+1}-\varphi_1 T_2-\delta_c\beta_1^{t+1}T_{bl,a}^{t+1}=\left(\frac{\zeta_c}{\Delta t}-\delta_c\beta_1^{t}-\varphi_1\right)T_1^{t}+\varphi_1 T_2+\delta_c\beta_1^{t}T_{bl,a}^{t}+\delta_c\left(q_{m,1}^{t+1}+q_{m,1}^{t}\right)$$

where

$$\zeta_c=\frac{4\pi r_1^3\left(\frac{1}{r_1}-\frac{1}{r_2}\right)}{3k_1}\rho_1 c_1,\ \delta_c=\frac{2\pi r_1^3\left(\frac{1}{r_1}-\frac{1}{r_2}\right)}{3k_1},\ \beta_1^t=q_{m,1}^t=0,\ \forall t,\ \varphi_1=2\pi \text{ and } \Delta t=300\ s.$$

For the 15th and imaginary node the skin boundary condition Eq. (4.25) is applied with $j\to 14$ *and* $(j+1)''\to 15$ as

$$\left[\frac{k_{14}}{r_{sk}^2\left(\frac{1}{r_{14}}-\frac{1}{r_{sk}}\right)}\left(1-\frac{r_{14}}{2r_{sk}}\right)-\frac{r_{14}}{2r_{sk}R_{lT}}\right]T_{14}-\left[\frac{r_{15}}{2r_{sk}}\left(\frac{k_{14}}{r_{sk}^2\left(\frac{1}{r_{14}}-\frac{1}{r_{sk}}\right)}+\frac{1}{R_{lT}}\right)\right]T_{15}=\frac{p_{sk}-p_{air}}{R_{e,lT}}-\frac{T_o}{R_{lT}},$$

with $R_{lT}=1/h,\quad R_{e,lT}=1/(L_a h),\quad p_{air}=RH\ p_{air,sat},\quad p_{sk}=\dfrac{\frac{p_{air}}{R_{e,lT}}+\lambda_{H^2O}\frac{1}{A_{sk}}\frac{dm_{sw}}{dt}+\frac{p_{s,sk}}{R_{e,sk}}}{\frac{1}{R_{e,lT}}+\frac{1}{R_{e,sk}}},$

$\dfrac{dm_{sw}}{dt}=0$ and $T_o=T_{air}=T_{mrt}=0\ ^oC$. Irradiation is switched off.

For every other *j* node the bioheat equation (4.8) is applied in spherical coordinates:

$$\begin{aligned}&\left(\gamma_j-1\right)T_{j-1}^{t+1}+\left(\frac{\zeta_j}{\Delta t}+2+\delta_j\beta_j^{t+1}\right)T_j^{t+1}-\left(\gamma_j+1\right)T_{j+1}^{t+1}-\delta_j\beta_j^{t+1}T_{bl,a}^{t+1}=\\&=\left(1-\gamma_j\right)T_{j-1}^{t}+\left(\frac{\zeta_j}{\Delta t}-2-\delta_j\beta_j^{t}\right)T_j^{t}+\left(\gamma_j+1\right)T_{j+1}^{t}+\delta_j\beta_j^{t}T_{bl,a}^{t}+\delta_j\left(q_{m,j}^{t+1}+q_{m,j}^{t}\right)\end{aligned},$$

with $\zeta_j = \rho_j c_j \frac{\Delta r_{j-1}^2 + \Delta r_j^2}{k_j}$, $\delta_j = \frac{\Delta r_{j-1}^2 + \Delta r_j^2}{2k_j}$, $\gamma_j = \frac{\omega}{2r_j} \frac{\Delta r_{j-1}^2 + \Delta r_j^2}{\Delta r_{j-1} + \Delta r_j}$, $\omega = 1$, $\Delta t = 300\ s$ and $\beta_1^t = q_{m,1}^t = 0,\ \forall t$.

A comparison between the calculated temperature values at the inner core node, the skin node and an interior node by the Fiala Model and the present work are presented in Table 5.5, Table 5.6 and Table 5.7 respectively. The interior node is at radius $r_{btw} = 0.075\ m$. For this test (depending on the mesh) is not necessary that there is a node at $r_{btw} = 0.075\ m$ so the temperature for that radius is calculated by Eq. (4.15) using the information of the nearest nodes 8 and 9 as

$$T_{r_{btw}} = \frac{r_9 T_{r_9} - r_8 T_{r_8}}{r_9 - r_8} + \frac{T_{r_8} - T_{r_9}}{\frac{r_{btw}}{r_8} - \frac{r_{btw}}{r_9}} \ .$$

The comparison of the present results with the analytic solution for sphere by Gröber and of the Fiala results with the same analytic solution [11] is presented in Figure 5.4.

This test has been conducted to verify the accuracy of the present work at the formulation of the equations in spherical coordinates and to partially test the code. More specifically, the accuracy of the following characteristics of the present work have been verified:

- the accuracy of the core boundary condition in spherical coordinates (for spheres)
- the accuracy of the outer skin boundary condition in spherical coordinates (for spheres)
- the heat transfer within a homogeneous tissue in spherical coordinates (for spheres)
- the transient temperature results for the equations discretized in spherical coordinates

For the inner core node temperatures, the comparison is presented in the table below

Time [hours]	**1**	**2**	**3**	**4**	**5**	**6**	**7**	**8**	**9**	**10**	**11**	**12**	**13**	**14**	**15**	**16**
Fiala Model [^oC]	35.98	31.45	25.84	20.71	16.42	13.03	10.29	8.08	6.35	5.01	3.96	3.09	2.43	1.96	1.61	1.13
Present Work [^oC]	36.38	31.84	25.86	20.45	16.01	12.49	9.73	7.57	5.89	4.58	3.56	2.76	2.14	1.66	1.29	0.99

Table 5.5 : Comparison of the inner core node temperature for single-layer spherical element test with corresponding results in [11]

Time [hours]	**1**	**2**	**3**	**4**	**5**	**6**	**7**	**8**	**9**	**10**	**11**	**12**	**13**	**14**	**15**	**16**
Fiala Model [^oC]	15.26	10.70	8.00	6.22	4.84	3.81	2.94	2.33	1.79	1.40	1.07	0.82	0.60	0.47	0.35	0.29
Present Work [^oC]	15.26	10.53	7.83	5.99	4.62	3.59	2.78	2.16	1.67	1.29	0.99	0.77	0.59	0.45	0.34	0.26

Table 5.6 : Comparison of outer skin temperature for single-layer spherical element test with corresponding results in [11

Time [hours]	**1**	**2**	**3**	**4**	**5**	**6**	**7**	**8**	**9**	**10**	**11**	**12**	**13**	**14**	**15**	**16**
Fiala Model [^oC]	30.67	23.35	18.06	14.12	11.11	8.68	6.88	5.42	4.25	3.28	2.62	1.96	1.52	1.22	0.93	0.72
Present Work [^oC]	29.73	22.12	16.91	13.07	10.15	7.88	6.13	4.77	3.71	2.88	2.24	1.73	1.34	1.03	0.8	0.61

Table 5.7 : Comparison of interior node temperature for single-layer spherical element test with corresponding results in [11]

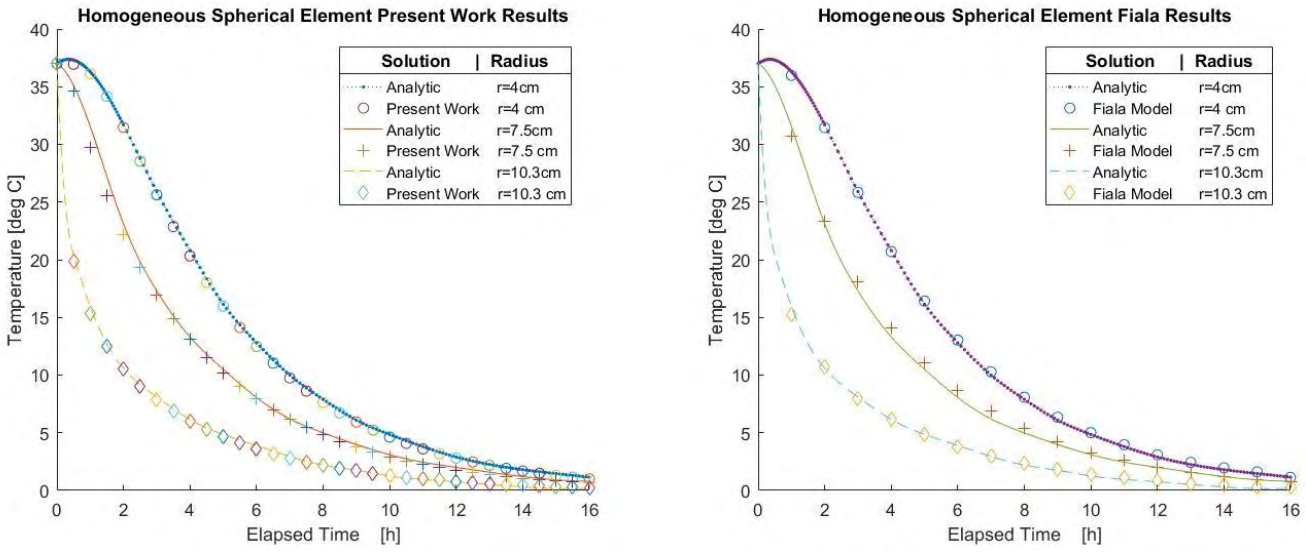

(a) (b)

Figure 5.4 : Comparison of the analytical results for a spherical element in [11] with (a) the present results and (b) the Fiala results

5.2 Multi-layer elements

Towards the aim of creating a model simulating the whole passive system of human body heat transfer, more tests must be conducted to verify and validate the present work. The next two tests regard the simulation of individual elements. These elements are simulated as multi-layer elements with all tissues and associated properties and data according to Table 2.3. In each case two simulations are made: one with an assumption of a steady and given blood pool temperature at 37^oC (Simulation A) and another one without this assumption where the blood pool temperature is part of the solution procedure (Simulation B). In both simulations the blood pool temperature is equal with the arterial blood temperature because the countercurrent heat exchange coefficient is zero ($h_x = 0$).

5.2.1 Spherical element: head

The head element is the only element in which the first layer outer radius, at 8.6 cm, is not considered to be the core radius. It is assumed that there is an inner core at 4 cm at which the temperature of the hypothalamus is calculated. To be more specific, a multilayer sphere – presented as head, with an outer radius of 10.4 cm, is exposed to an environment with neutral conditions according to Table 3.2 and the metabolic heat produced is equal to the basal one. The layers are made up as follows: the first layer by the brain tissue with outer radius of 8.6 cm, the second layer by the bone tissue with outer radius of 10.05 cm, the third and fourth layers by the fat and skin tissues with outer radius at 10.2 and 10.4 cm respectively. The tissue and node properties and factors are given in Table 2.3. In Figure 5.5 the head element with all nodes (regular and fictitious) are presented in detail. The sequence of layers and nodes is exact, but the ratios are not for intelligibility reasons.

Next, it is useful to present in detail which equations is applied to each node. The first layer of the element is the brain layer.

The first node is the core node located at the inner core interface. For this node Eq. (4.19) is applied for spherical coordinates with $j \to 1,\ jnext,1 \to 2,\ jnext,2 \to 21.$

$$\left(\frac{\zeta_c}{\Delta t}+\delta_c\beta_1^{t+1}+\left(\varphi_1+\varphi_2\right)\right)T_1^{t+1}-\left(\varphi_1 T_2^{t+1}+\varphi_2 T_{21}^{t+1}\right)-\delta_c\beta_1^{t+1}T_{bl,a}^{t+1}=$$
$$=\left(\frac{\zeta_c}{\Delta t}-\delta_c\beta_1^{t}-\left(\varphi_1+\varphi_2\right)\right)T_1^{t}+\left(\varphi_1 T_2^{t}+\varphi_2 T_{21}^{t}\right)+\delta_c\beta_1^{t}T_{bl,a}^{t}+\delta_c\left(q_{m,1}^{t+1}+q_{m,1}^{t}\right),$$

with $\zeta_c=\dfrac{4\pi r_1^3\left(\dfrac{1}{r_1}-\dfrac{1}{r_2}\right)}{3k_1}\rho_1 c_1,\quad \delta_c=\dfrac{2\pi r_1^3\left(\dfrac{1}{r_1}-\dfrac{1}{r_2}\right)}{3k_1},\quad \Delta t=60\ s,\quad k_1=0.49 W/(m\,K),$

$c_1=3850\ J/(kg\,K),\ \ \rho_1=1080\,kg/m^3,\ \ w_{bl,0,1}=10.1320\cdot 10^{-3}\ s^{-1}, q_{m,1}=13400\,W/m^3,$

$\varphi_1=\pi/18$ and $\varphi_1=17\pi/18$.

For nodes 2, 3, 4, 5, 21, 22, 23, 24 the bioheat equation (4.8) for spherical coordinates is applied for $j \to 2,3,4,5,21,22,23,24$ as

$$\left(\gamma_j-1\right)T_{j-1}^{t+1}+\left(\frac{\zeta_j}{\Delta t}+2+\delta_j\beta_j^{t+1}\right)T_j^{t+1}-\left(\gamma_j+1\right)T_{j+1}^{t+1}-\delta_j\beta_j^{t+1}T_{bl,a}^{t+1}=$$
$$=\left(1-\gamma_j\right)T_{j-1}^{t}+\left(\frac{\zeta_j}{\Delta t}-2-\delta_j\beta_j^{t}\right)T_j^{t}+\left(\gamma_j+1\right)T_{j+1}^{t}+\delta_j\beta_j^{t}T_{bl,a}^{t}+\delta_j\left(q_{m,j}^{t+1}+q_{m,j}^{t}\right)$$

with $\zeta_j=\rho_j c_j\dfrac{\Delta r_{j-1}^2+\Delta r_j^2}{k_j},\ \ \delta_j=\dfrac{\Delta r_{j-1}^2+\Delta r_j^2}{2k_j},\ \gamma_j=\dfrac{\omega}{2r_j}\dfrac{\Delta r_{j-1}^2+\Delta r_j^2}{\Delta r_{j-1}+\Delta r_j},\ \ \omega=2,\ \ k_j=0.49 W/(m\,K),$

$\rho_j=1080\,kg/m^3,\ \ c_j=3850\ J/(kg\,K),\ \ w_{bl,0,j}=10.1320\cdot 10^{-3}\ s^{-1}, q_{m,j}=13400\,W/m^3$

For nodes 6, 25 the first interface boundary equation (4.14) is applied with $j \to 5,24,\ (j+1)'' \to 6,25,\ \ j'' \to 7,26,\ (j+1) \to 8,27$ as

$$k_5\frac{T_5-T_6}{\frac{1}{r_6}-\frac{1}{r_5}}=k_8\frac{T_7-T_8}{\frac{1}{r_8}-\frac{1}{r_7}} \qquad k_{24}\frac{T_{24}-T_{25}}{\frac{1}{r_{25}}-\frac{1}{r_{24}}}=k_{27}\frac{T_{26}-T_{27}}{\frac{1}{r_{27}}-\frac{1}{r_{26}}}$$

For nodes 7, 26 the second interface boundary equation (4.16) is applied and again $j\to 5,24,\ (j+1)''\to 6,25,\quad j''\to 7,26,\ (j+1)\to 8,27$ respectively.

$$\frac{r_6T_6-r_5T_5}{r_6-r_5}+\frac{T_5-T_6}{\frac{r_{ifc}}{r_5}-\frac{r_{ifc}}{r_6}}=T_{ifc}=\frac{r_8T_8-r_7T_7}{r_8-r_7}+\frac{T_7-T_8}{\frac{r_{ifc}}{r_7}-\frac{r_{ifc}}{r_8}}$$

$$\frac{r_{14}T_{14}-r_{13}T_{13}}{r_{14}-r_{13}}+\frac{T_{13}-T_{14}}{\frac{r_{ifc}}{r_{13}}-\frac{r_{ifc}}{r_{14}}}=T_{ifc}=\frac{r_{16}T_{16}-r_{15}T_{15}}{r_{16}-r_{15}}+\frac{T_{15}-T_{16}}{\frac{r_{ifc}}{r_{15}}-\frac{r_{ifc}}{r_{16}}}$$

For nodes 8, 9, 27, 28 the bioheat equation (4.8) is applied with $j\to 8,9,27,28$.

$$\left(\gamma_j-1\right)T_{j-1}^{t+1}+\left(\frac{\zeta_j}{\Delta t}+2+\delta_j\beta_j^{t+1}\right)T_j^{t+1}-\left(\gamma_j+1\right)T_{j+1}^{t+1}-\delta_j\beta_j^{t+1}T_{bl,a}^{t+1}=$$

$$=\left(1-\gamma_j\right)T_{j-1}^{t}+\left(\frac{\zeta_j}{\Delta t}-2-\delta_j\beta_j^{t}\right)T_j^{t}+\left(\gamma_j+1\right)T_{j+1}^{t}+\delta_j\beta_j^{t}T_{bl,a}^{t}+\delta_j\left(q_{m,j}^{t+1}+q_{m,j}^{t}\right)$$

with $\zeta_j=\rho_jc_j\frac{\Delta r_{j-1}^2+\Delta r_j^2}{k_j},\ \delta_j=\frac{\Delta r_{j-1}^2+\Delta r_j^2}{2k_j},\ \gamma_j=\frac{\omega}{2r_j}\frac{\Delta r_{j-1}^2+\Delta r_j^2}{\Delta r_{j-1}+\Delta r_j},\ \omega=2,\ k_j=1.16W/(mK),$

$\rho_j=1500\,kg/m^3,\ c_j=1591\ J/(kg\,K),\ w_{bl,0,j}=0,\ q_{m,j}=0$

For nodes 10, 29, Eq. (4.14) is applied with $j\to 9,28,\ (j+1)''\to 10,29,$ $j''\to 11,30,\ (j+1)\to 12,31$.

$$k_9\frac{T_9-T_{10}}{\frac{1}{r_{10}}-\frac{1}{r_9}}=k_{12}\frac{T_{11}-T_{12}}{\frac{1}{r_{12}}-\frac{1}{r_{11}}} \qquad k_{28}\frac{T_{28}-T_{29}}{\frac{1}{r_{29}}-\frac{1}{r_{28}}}=k_{31}\frac{T_{30}-T_{31}}{\frac{1}{r_{31}}-\frac{1}{r_{30}}}$$

For nodes 11, 30, Eq. (4.16) is applied for $j \to 9, 28,\ (j+1)'' \to 10, 29,$ $j'' \to 11, 30,\ (j+1) \to 12, 31$.

$$\frac{r_{10}T_{10} - r_9 T_9}{r_{10} - r_9} + \frac{T_9 - T_{10}}{\frac{r_{ifc}}{r_9} - \frac{r_{ifc}}{r_{10}}} = T_{ifc} = \frac{r_{12}T_{12} - r_{11}T_{11}}{r_{12} - r_{11}} + \frac{T_{11} - T_{12}}{\frac{r_{ifc}}{r_{11}} - \frac{r_{ifc}}{r_{12}}}$$

$$\frac{r_{29}T_{29} - r_{28}T_{28}}{r_{29} - r_{28}} + \frac{T_{28} - T_{29}}{\frac{r_{ifc}}{r_{28}} - \frac{r_{ifc}}{r_{29}}} = T_{ifc} = \frac{r_{31}T_{31} - r_{30}T_{30}}{r_{31} - r_{30}} + \frac{T_{30} - T_{31}}{\frac{r_{ifc}}{r_{30}} - \frac{r_{ifc}}{r_{31}}}$$

For nodes 12, 13, 31, 32, Eq. (4.8) is applied for $j = 12, 13, 31, 32$

$$\left(\gamma_j - 1\right)T_{j-1}^{t+1} + \left(\frac{\zeta_j}{\Delta t} + 2 + \delta_j \beta_j^{t+1}\right)T_j^{t+1} - \left(\gamma_j + 1\right)T_{j+1}^{t+1} - \delta_j \beta_j^{t+1} T_{bl,a}^{t+1} =$$

$$= \left(1 - \gamma_j\right)T_{j-1}^{t} + \left(\frac{\zeta_j}{\Delta t} - 2 - \delta_j \beta_j^{t}\right)T_j^{t} + \left(\gamma_j + 1\right)T_{j+1}^{t} + \delta_j \beta_j^{t} T_{bl,a}^{t} + \delta_j \left(q_{m,j}^{t+1} + q_{m,j}^{t}\right)$$

with $\zeta_j = \rho_j c_j \frac{\Delta r_{j-1}^2 + \Delta r_j^2}{k_j}$, $\delta_j = \frac{\Delta r_{j-1}^2 + \Delta r_j^2}{2k_j}$, $\gamma_j = \frac{\omega}{2r_j} \frac{\Delta r_{j-1}^2 + \Delta r_j^2}{\Delta r_{j-1} + \Delta r_j}$, $\omega = 2$, $k_j = 0.16 W/(m\,K)$,

$\rho_j = 850\, kg/m^3$, $c_j = 2300\ J/(kg\,K)$, $w_{bl,0,j} = 0.0036 \cdot 10^{-3}\, s^{-1}$, $q_{m,j} = 58\ W/m^3$

For nodes 14, 33, Eq. (4.14) is applied for $j \to 13, 32,\ (j+1)'' \to 14, 33,$ $j'' \to 15, 34,\ (j+1) \to 16, 35$.

$$k_{13} \frac{T_{13} - T_{14}}{\frac{1}{r_{14}} - \frac{1}{r_{13}}} = k_{16} \frac{T_{15} - T_{16}}{\frac{1}{r_{16}} - \frac{1}{r_{15}}} \qquad k_{32} \frac{T_{32} - T_{33}}{\frac{1}{r_{33}} - \frac{1}{r_{32}}} = k_{35} \frac{T_{34} - T_{35}}{\frac{1}{r_{35}} - \frac{1}{r_{34}}}$$

For nodes 15, 34, Eq. (4.16) is applied for $j \to 13, 32,\ (j+1)'' \to 14, 33,$ $j'' \to 15, 34,\ (j+1) \to 16, 35$.

$$\frac{r_{14}T_{14}-r_{13}T_{13}}{r_{14}-r_{13}}+\frac{T_{13}-T_{14}}{\frac{r_{ifc}}{r_{13}}-\frac{r_{ifc}}{r_{14}}}=T_{ifc}=\frac{r_{16}T_{16}-r_{15}T_{15}}{r_{16}-r_{15}}+\frac{T_{15}-T_{16}}{\frac{r_{ifc}}{r_{15}}-\frac{r_{ifc}}{r_{16}}}$$

$$\frac{r_{33}T_{33}-r_{32}T_{32}}{r_{33}-r_{32}}+\frac{T_{32}-T_{33}}{\frac{r_{ifc}}{r_{32}}-\frac{r_{ifc}}{r_{33}}}=T_{ifc}=\frac{r_{35}T_{35}-r_{34}T_{34}}{r_{35}-r_{34}}+\frac{T_{34}-T_{35}}{\frac{r_{ifc}}{r_{34}}-\frac{r_{ifc}}{r_{35}}}$$

For nodes 16, 17, 18, 19, 35, 36, 37, 38, Eq. (4.8) is applied for $j\rightarrow 16,\ 17,\ 18,\ 19,\ 35,\ 36,\ 37,\ 38$.

$$\left(\gamma_j-1\right)T_{j-1}^{t+1}+\left(\frac{\zeta_j}{\Delta t}+2+\delta_j\beta_j^{t+1}\right)T_j^{t+1}-\left(\gamma_j+1\right)T_{j+1}^{t+1}-\delta_j\beta_j^{t+1}T_{bl,a}^{t+1}=$$
$$=\left(1-\gamma_j\right)T_{j-1}^{t}+\left(\frac{\zeta_j}{\Delta t}-2-\delta_j\beta_j^{t}\right)T_j^{t}+\left(\gamma_j+1\right)T_{j+1}^{t}+\delta_j\beta_j^{t}T_{bl,a}^{t}+\delta_j\left(q_{m,j}^{t+1}+q_{m,j}^{t}\right)$$

with $\zeta_j=\rho_j c_j\frac{\Delta r_{j-1}^2+\Delta r_j^2}{k_j}$, $\delta_j=\frac{\Delta r_{j-1}^2+\Delta r_j^2}{2k_j}$, $\gamma_j=\frac{\omega}{2r_j}\frac{\Delta r_{j-1}^2+\Delta r_j^2}{\Delta r_{j-1}+\Delta r_j}$, $\omega=2$, $k_j=0.47W/(mK)$,

$\rho_j=1085\,kg/m^3$, $c_j=3680\ J/(kg\,K)$, $w_{bl,0,j}=5.48\cdot10^{-3}\,s^{-1}$, $q_{m,j}=368\ W/m^3$.

Then, for nodes 20, 39 the skin boundary condition for spherical elements Eq. (4.25) is applied with $j\rightarrow 19,38$ *and* $(j+1)''\rightarrow 20,39$.

$$\left[\frac{k_{19}}{r_{sk}^2\left(\frac{1}{r_{19}}-\frac{1}{r_{sk}}\right)}\left(1-\frac{r_{19}}{2r_{sk}}\right)-\frac{r_{19}}{2r_{sk}R_{lT}}\right]T_{19}\ -\ \left[\frac{r_{20}}{2r_{sk}}\left(\frac{k_{19}}{r_{sk}^2\left(\frac{1}{r_{19}}-\frac{1}{r_{sk}}\right)}+\frac{1}{R_{lT}}\right)\right]T_{20}=\frac{p_{sk}-p_{air}}{R_{e,lT}}-\frac{T_o}{R_{lT}}$$

$$\left[\frac{k_{38}}{r_{sk}^2\left(\frac{1}{r_{38}}-\frac{1}{r_{sk}}\right)}\left(1-\frac{r_{38}}{2r_{sk}}\right)-\frac{r_{38}}{2r_{sk}R_{lT}}\right]T_{j}\ -\ \left[\frac{r_{39}}{2r_{sk}}\left(\frac{k_{38}}{r_{sk}^2\left(\frac{1}{r_{38}}-\frac{1}{r_{sk}}\right)}+\frac{1}{R_{lT}}\right)\right]T_{39}=\frac{p_{sk}-p_{air}}{R_{e,lT}}-\frac{T_o}{R_{lT}}$$

Finally, the 40th equation that completes the linear equation system Eq. (4.28) is applied for the blood pool temperature $T_{bl,p}$ as

$$\sum_{e}^{1}\left(\frac{\sum_{j}^{38}\beta_{e,j}V_{e,j}}{h_{x,e}+\sum_{j}^{38}\beta_{e,j}V_{e,j}}\cdot\sum_{j}^{38}\beta_{e,j}V_{e,j}T_{e,j}\right)-\sum_{e}^{1}\left(\frac{\left(\sum_{j}^{38}\beta_{e,j}V_{e,j}\right)^{2}}{h_{x,e}+\sum_{j}^{38}\beta_{e,j}V_{e,j}}\right)T_{bl,p}=0\ ,$$

where only the regular nodes are considered for this equation.

The code converges well in both simulations A and B. When the blood pool temperature ($T_{bl,p}$) is part of the solution (Simulation B) the time elapsed untill steady state conditions are obtained is larger than the corresponding one when the steady blood temperature $T_{bl,p}=37^{o}C$ is assumed (Simulation A). In Table 5.8 and Table 5.9 the steady state temperatures of all nodes for both simulations are presented while in Table 5.9 the steady state steady state blood pool temperature for the Simulation B is also presented.

It is noticed that the temperatures in Simulation B are unnaturally high but this is due to the fact that the brain tissue, according to the model, produces a great value of basal metabolic heat of 13400 W/m^{3}. It is expected that when the passive model of the whole body is considered the temperatures will be significantly lower. It is important, to note that in a simulation with a regular basal heat productivity into the brain tissue the temperatures are constantly decreasing and if the basal heat productivity is completely switched off the temperatures are steeply decreasing.

For further clarification, the results of the transient heat transfer problem for three head points are shown in Figure 5.6 for both Simulations A and B. The three head points are the hypothalamus (core node) at $r=4cm$, the node N=9 at $r\simeq 9.688cm$, which is the last bone

node at the forehead sector and the skin surface node, which since it is not a mesh node, it is calculated by the Eq. (4.15) for the skin outer radius using the information of nodes N=38 and N=39.

HEAD									
$T_{bl,p}$ **imposed at 37** ^oC									
Sector: Forehead					**Sector: Head**				
Node	Radius [cm]	Tissue	Temp. [^oC]	Comm.	Node	Radius [cm]	Tissue	Temp. [^oC]	Comm.
1	4,000	Brain	37,02	Thy	**1**	4,000	Brain	37,02	Thy
2	5,022	Brain	37,31		**21**	5,022	Brain	37,31	
3	6,044	Brain	37,34		**22**	6,044	Brain	37,34	
4	7,067	Brain	37,33		**23**	7,067	Brain	37,33	
5	8,089	Brain	37,24		**24**	8,089	Brain	37,25	
6	9,111	Brain	36,46	Imaginary	**25**	9,111	Brain	36,56	Imaginary
7	8,238	Bone	36,96	Imaginary	**26**	8,238	Bone	37,00	Imaginary
8	8,963	Bone	36,73		**27**	8,963	Bone	36,79	
9	9,688	Bone	36,53		**28**	9,688	Bone	36,61	
10	10,413	Bone	36,35	Imaginary	**29**	10,413	Bone	36,46	Imaginary
11	10,013	Fat	36,50	Imaginary	**30**	10,013	Fat	36,59	Imaginary
12	10,088	Fat	36,37		**31**	10,088	Fat	36,48	
13	10,163	Fat	36,25		**32**	10,163	Fat	36,37	
14	10,238	Fat	36,12	Imaginary	**33**	10,238	Fat	36,25	Imaginary
15	10,175	Skin	36,20	Imaginary	**34**	10,175	Skin	36,32	Imaginary
16	10,225	Skin	36,17		**35**	10,225	Skin	36,30	
17	10,275	Skin	36,13		**36**	10,275	Skin	36,26	
18	10,325	Skin	36,09		**37**	10,325	Skin	36,22	
19	10,375	Skin	36,03		**38**	10,375	Skin	36,17	
20	10,425	Skin	35,96	Imaginary	**39**	10,425	Skin	36,11	Imaginary
	10,4	Skin	35,99	T_{sk}		10,4	Skin	36,14	T_{sk}

Table 5.8 : Steady state temperature distribution of the head (Simulation A)

HEAD									
$T_{bl,p}$ **Part of Solution Procedure**									
Sector: Forehead					**Sector: Head**				
Node	Radius [cm]	Tissue	Temp. [^oC]	Comm.	**Node**	Radius [cm]	Tissue	Temp. [^oC]	Comm.
1	4,000	Brain	56,15	Thy	**1**	4,000	Brain		Thy
2	5,022	Brain	56,44		**21**	5,022	Brain	56,44	
3	6,044	Brain	56,46		**22**	6,044	Brain	56,46	
4	7,067	Brain	56,43		**23**	7,067	Brain	56,43	
5	8,089	Brain	56,13		**24**	8,089	Brain	56,17	
6	9,111	Brain	53,42	Imaginary	**25**	9,111	Brain	53,78	Imaginary
7	8,238	Bone	55,15	Imaginary	**26**	8,238	Bone	55,31	Imaginary
8	8,963	Bone	54,34		**27**	8,963	Bone	54,59	
9	9,688	Bone	53,65		**28**	9,688	Bone	53,98	
10	10,413	Bone	53,06	Imaginary	**29**	10,413	Bone	53,46	Imaginary
11	10,013	Fat	53,57	Imaginary	**30**	10,013	Fat	53,91	Imaginary
12	10,088	Fat	53,13		**31**	10,088	Fat	53,52	
13	10,163	Fat	52,69		**32**	10,163	Fat	53,13	
14	10,238	Fat	52,25	Imaginary	**33**	10,238	Fat	52,75	Imaginary
15	10,175	Skin	52,52	Imaginary	**34**	10,175	Skin	52,98	Imaginary
16	10,225	Skin	52,42		**35**	10,225	Skin	52,90	
17	10,275	Skin	52,28		**36**	10,275	Skin	52,77	
18	10,325	Skin	52,10		**37**	10,325	Skin	52,62	
19	10,375	Skin	51,87		**38**	10,375	Skin	52,42	
20	10,425	Skin	51,60	Imaginary	**39**	10,425	Skin	52,18	Imaginary
	10,4	Skin	51,74	*Tsk*		10,4	Skin	52,30	*Tsk*
			56,12	$T_{bl,p}$				56,12	$T_{bl,p}$

Table 5.9 : Steady state temperature distribution of the head (Simulation B)

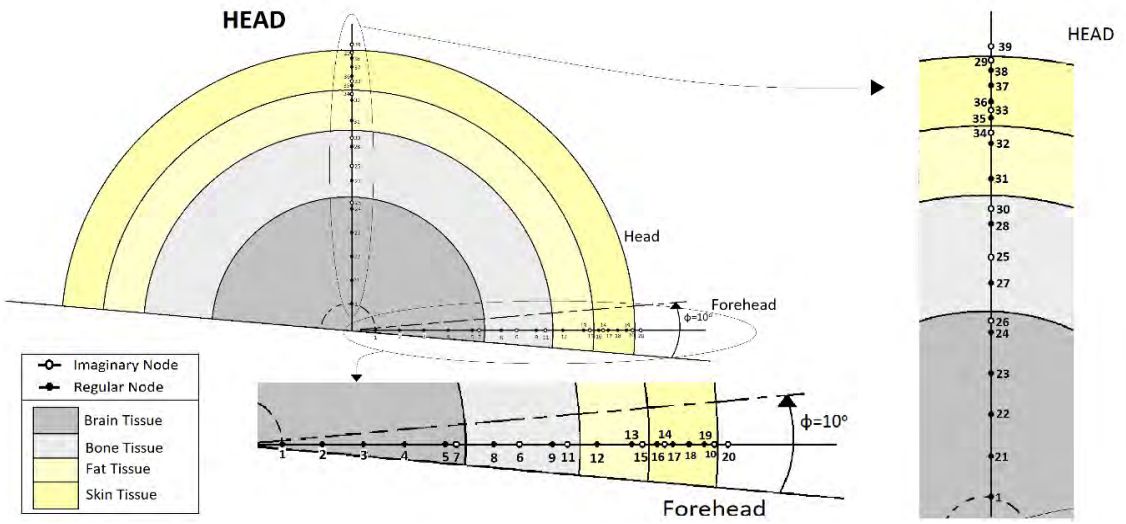

Figure 5.6 : Schematic view of the head element

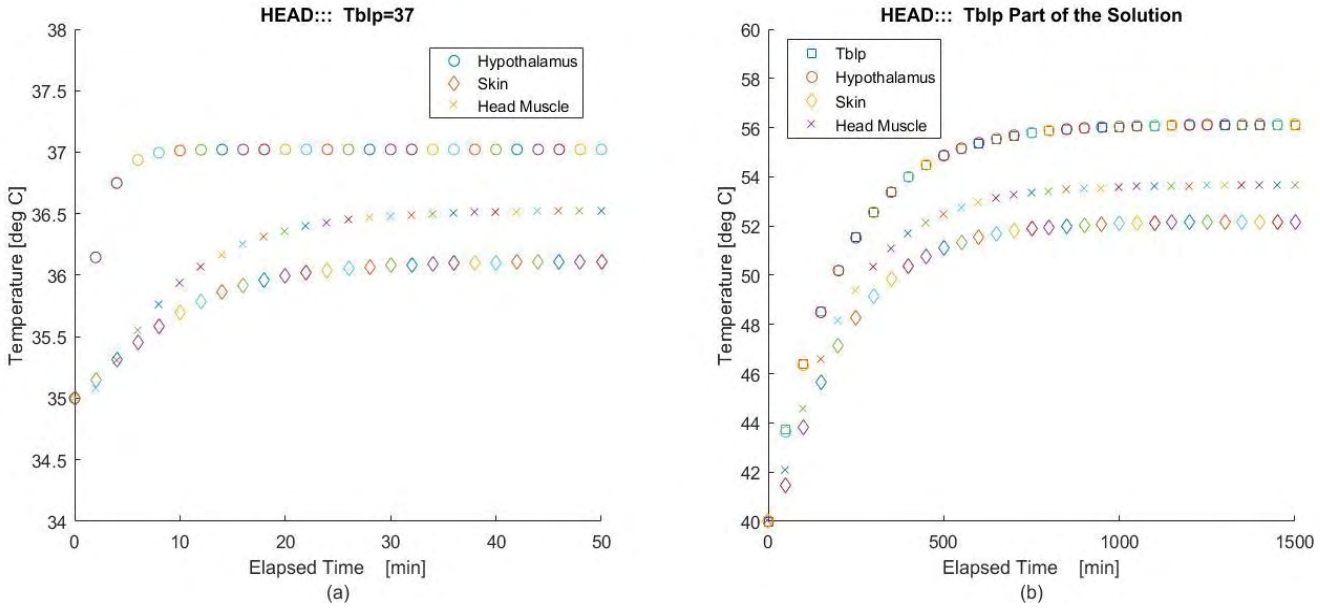

Figure 5.5 : Temperatures at three head nodes: (a) Simulation A and (b) Simulation B

5.2.2 Cylindrical element: neck

The second individual body element to be considered is the neck cylindrical element using all required data according to the Fiala Model, presented in Table 2.3. The neck-element is exposed in neutral conditions i.e. air temperature, radiation temperature, relative humidity, air speed, activity level and emissivity of the wall surfaces according to Table 3.2. The cylinder has an outer radius at 5.67 cm representing skin and its inner core is at 1.9 cm, which is also the outer bone radius. There are four layers (bone, muscle, fat and skin) two sectors (anterior and posterior) and 35 nodes. The nodes are distributed as follows: each of the two sectors have 17 nodes plus 1 common node, the core node, which is assumed to have uniform temperature. From the 17 nodes the 11 are regular and 6 are fictitious. More information for the node distribution is shown in Figure 4.4, where although the sequence of the layers and nodes is exact, the ratios are not for intelligibility reasons. Information about the nodes and radiuses are shown in Table 5.10 and Table 2.3.

Next, the detailed description of the equations used for each node of the neck element is presented. The first node is the core node and is common for both sectors. For this node Eq. (4.19) is applied, with $j \to 1,\ jnext,1 \to 2,\ jnext,2 \to 19$.

$$\left(\frac{\zeta_c}{\Delta t}+\delta_c\beta_1^{t+1}+\left(\varphi_1+\varphi_2\right)\right)T_1^{t+1}-\left(\varphi_1 T_2^{t+1}+\varphi_2 T_{19}^{t+1}\right)-\delta_c\beta_1^{t+1}T_{bl,a}^{t+1}=$$
$$=\left(\frac{\zeta_c}{\Delta t}-\delta_c\beta_1^{t}-\left(\varphi_1+\varphi_2\right)\right)T_1^{t}+\left(\varphi_1 T_2^{t}+\varphi_2 T_{19}^{t}\right)+\delta_c\beta_1^{t}T_{bl,a}^{t}+\delta_c\left(q_{m,1}^{t+1}+q_{m,1}^{t}\right),$$

with $\zeta_c=\dfrac{2\pi r_j^2\ln\left(\dfrac{r_{jnext,s=1}}{r_j}\right)}{k_j}\rho_j c_j$, $\delta_c=\dfrac{\pi r_j^2\ln\left(\dfrac{r_{jnext,s=1}}{r_j}\right)}{k_j}$, $\Delta t=60\ s$, $\varphi_1=\pi/2$, $\varphi_2=\pi/2$,

while $k_j,\ \rho_j, c_j, w_{bl,0,j},\ q_{m,bas,0,j}$ are given in Table 2.3 for neck bone tissue.

For nodes 2, 19 the first interface boundary condition Eq. (4.10) is applied with

$j \to 1,1,\ (j+1)'' \to 2,19,\quad j'' \to 3,20,\ (j+1) \to 4,21$

$$k_1 \frac{(T_2 - T_1)}{\ln\left(\frac{r_2}{r_1}\right)} = k_4 \frac{(T_4 - T_3)}{\ln\left(\frac{r_4}{r_3}\right)} \qquad k_1 \frac{(T_{19} - T_1)}{\ln\left(\frac{r_{19}}{r_1}\right)} = k_{20} \frac{(T_{20} - T_{21})}{\ln\left(\frac{r_{20}}{r_{21}}\right)}$$

For nodes 3, 20 the second interface boundary condition Eq. (4.12) is applied with

$j \to 1,1,\ (j+1)'' \to 2,19,\quad j'' \to 3,20,\ (j+1) \to 4,21$

$$\frac{T_1 \ln\left(\frac{r_{ifc}}{r_2}\right) - T_2 \ln\left(\frac{r_{ifc}}{r_1}\right)}{\ln\left(\frac{r_1}{r_2}\right)} = T_{ifc} = \frac{T_3 \ln\left(\frac{r_{ifc}}{r_4}\right) - T_4 \ln\left(\frac{r_{ifc}}{r_3}\right)}{\ln\left(\frac{r_3}{r_4}\right)}$$

$$\frac{T_1 \ln\left(\frac{r_{ifc}}{r_{19}}\right) - T_{19} \ln\left(\frac{r_{ifc}}{r_1}\right)}{\ln\left(\frac{r_1}{r_{19}}\right)} = T_{ifc} = \frac{T_{20} \ln\left(\frac{r_{ifc}}{r_{21}}\right) - T_{21} \ln\left(\frac{r_{ifc}}{r_{20}}\right)}{\ln\left(\frac{r_{20}}{r_{21}}\right)}$$

For nodes 4, 5, 6, 7, 21, 22, 23, 24 the bioheat equation (4.8) is applied and $j \to 4,\ 5,\ 6,\ 7,\ 21,\ 22,\ 23,\ 24.$

$$\left(\gamma_j - 1\right) T_{j-1}^{t+1} + \left(\frac{\zeta_j}{\Delta t} + 2 + \delta_j \beta_j^{t+1}\right) T_j^{t+1} - \left(\gamma_j + 1\right) T_{j+1}^{t+1} - \delta_j \beta_j^{t+1} T_{bl,a}^{t+1} =$$

$$= \left(1 - \gamma_j\right) T_{j-1}^{t} + \left(\frac{\zeta_j}{\Delta t} - 2 - \delta_j \beta_j^{t}\right) T_j^{t} + \left(\gamma_j + 1\right) T_{j+1}^{t} + \delta_j \beta_j^{t} T_{bl,a}^{t} + \delta_j \left(q_{m,j}^{t+1} + q_{m,j}^{t}\right),$$

with $\zeta_j = \rho_j c_j \frac{\Delta r_{j-1}^2 + \Delta r_j^2}{k_j}$, $\delta_j = \frac{\Delta r_{j-1}^2 + \Delta r_j^2}{2k_j}$, $\gamma_j = \frac{\omega}{2r_j} \frac{\Delta r_{j-1}^2 + \Delta r_j^2}{\Delta r_{j-1} + \Delta r_j}$, $\omega = 1,$

while $\rho_j, c_j, w_{bl,0,j}$, $q_{m,bas,0,j}$ are obtained from Table 2.3 for neck muscle tissue.

For nodes 8, 25, Eq. (4.10) is applied with $j \to 7, 24, \left(j+1\right)'' \to 8, 25,$ $j'' \to 9, 26, \left(j+1\right) \to 10, 27$ as

$$k_7 \frac{\left(T_8 - T_7\right)}{\ln\left(\frac{r_8}{r_7}\right)} = k_{10} \frac{\left(T_{10} - T_9\right)}{\ln\left(\frac{r_{10}}{r_9}\right)} \qquad k_{24} \frac{\left(T_{25} - T_{24}\right)}{\ln\left(\frac{r_{25}}{r_{24}}\right)} = k_{27} \frac{\left(T_{27} - T_{26}\right)}{\ln\left(\frac{r_{27}}{r_{26}}\right)}$$

For nodes 9, 26, Eq. (4.12) is applied with $j \to 7, 24, \left(j+1\right)'' \to 8, 25,$ $j'' \to 9, 26, \left(j+1\right) \to 10, 27$

$$\frac{T_7 \ln\left(\frac{r_{ifc}}{r_8}\right) - T_8 \ln\left(\frac{r_{ifc}}{r_7}\right)}{\ln\left(\frac{r_7}{r_8}\right)} = T_{ifc} = \frac{T_9 \ln\left(\frac{r_{ifc}}{r_{10}}\right) - T_{10} \ln\left(\frac{r_{ifc}}{r_9}\right)}{\ln\left(\frac{r_9}{r_{10}}\right)}$$

$$\frac{T_{24} \ln\left(\frac{r_{ifc}}{r_{25}}\right) - T_{25} \ln\left(\frac{r_{ifc}}{r_{24}}\right)}{\ln\left(\frac{r_{24}}{r_{25}}\right)} = T_{ifc} = \frac{T_{26} \ln\left(\frac{r_{ifc}}{r_{27}}\right) - T_{27} \ln\left(\frac{r_{ifc}}{r_{26}}\right)}{\ln\left(\frac{r_{26}}{r_{27}}\right)}$$

For nodes 10, 11, 28, 29, the bioheat equation (4.8) is applied with $j \to 10,\ 11,\ 28,\ 29$

.

$$\left(\gamma_j - 1\right) T_{j-1}^{t+1} + \left(\frac{\zeta_j}{\Delta t} + 2 + \delta_j \beta_j^{t+1}\right) T_j^{t+1} - \left(\gamma_j + 1\right) T_{j+1}^{t+1} - \delta_j \beta_j^{t+1} T_{bl,a}^{t+1} =$$

$$= \left(1 - \gamma_j\right) T_{j-1}^{t} + \left(\frac{\zeta_j}{\Delta t} - 2 - \delta_j \beta_j^{t}\right) T_j^{t} + \left(\gamma_j + 1\right) T_{j+1}^{t} + \delta_j \beta_j^{t} T_{bl,a}^{t} + \delta_j \left(q_{m,j}^{t+1} + q_{m,j}^{t}\right),$$

with $\zeta_j = \rho_j c_j \frac{\Delta r_{j-1}^2 + \Delta r_j^2}{k_j}, \delta_j = \frac{\Delta r_{j-1}^2 + \Delta r_j^2}{2k_j}, \gamma_j = \frac{\omega}{2r_j} \frac{\Delta r_{j-1}^2 + \Delta r_j^2}{\Delta r_{j-1} + \Delta r_j}, \omega = 1,$

while $\rho_j, c_j, w_{bl,0,j}, q_{m,bas,0,j}$ are obtained from Table 2.3 for neck fat tissue.

For nodes 12, 29, Eq. (4.10) is applied using $j \to 11,28,\ (j+1)'' \to 12,29,$ $j'' \to 13,30,\ (j+1) \to 14,31$

$$k_{11}\frac{(T_{12}-T_{11})}{\ln\left(\frac{r_{12}}{r_{11}}\right)} = k_{14}\frac{(T_{14}-T_{13})}{\ln\left(\frac{r_{14}}{r_{13}}\right)} \qquad k_{28}\frac{(T_{29}-T_{28})}{\ln\left(\frac{r_{29}}{r_{28}}\right)} = k_{31}\frac{(T_{31}-T_{30})}{\ln\left(\frac{r_{31}}{r_{30}}\right)}$$

For nodes 13, 30, Eq. (4.12) is applied with $j \to 11,28,\ (j+1)'' \to 12,29,$ $j'' \to 13,30,\ (j+1) \to 14,31$

$$\frac{T_{11}\ln\left(\frac{r_{ifc}}{r_{12}}\right)-T_{12}\ln\left(\frac{r_{ifc}}{r_{11}}\right)}{\ln\left(\frac{r_{11}}{r_{12}}\right)} = T_{ifc} = \frac{T_{13}\ln\left(\frac{r_{ifc}}{r_{14}}\right)-T_{14}\ln\left(\frac{r_{ifc}}{r_{13}}\right)}{\ln\left(\frac{r_{13}}{r_{14}}\right)}$$

$$\frac{T_{28}\ln\left(\frac{r_{ifc}}{r_{29}}\right)-T_{29}\ln\left(\frac{r_{ifc}}{r_{28}}\right)}{\ln\left(\frac{r_{28}}{r_{29}}\right)} = T_{ifc} = \frac{T_{30}\ln\left(\frac{r_{ifc}}{r_{31}}\right)-T_{31}\ln\left(\frac{r_{ifc}}{r_{30}}\right)}{\ln\left(\frac{r_{30}}{r_{31}}\right)}$$

For nodes 14, 15, 16, 17, 31, 32, 33, 34, Eq. (4.8) is applied with $j \to 14,\ 15,\ 16,\ 17,\ 31,\ 32,\ 33,\ 34.$

$$\left(\gamma_j - 1\right)T_{j-1}^{t+1} + \left(\frac{\zeta_j}{\Delta t} + 2 + \delta_j\beta_j^{t+1}\right)T_j^{t+1} - \left(\gamma_j + 1\right)T_{j+1}^{t+1} - \delta_j\beta_j^{t+1}T_{bl,a}^{t+1} =$$
$$= \left(1-\gamma_j\right)T_{j-1}^{t} + \left(\frac{\zeta_j}{\Delta t} - 2 - \delta_j\beta_j^{t}\right)T_j^{t} + \left(\gamma_j + 1\right)T_{j+1}^{t} + \delta_j\beta_j^{t}T_{bl,a}^{t} + \delta_j\left(q_{m,j}^{t+1} + q_{m,j}^{t}\right),$$

with $\zeta_j = \rho_j c_j \frac{\Delta r_{j-1}^2 + \Delta r_j^2}{k_j}$, $\gamma_j = \frac{\omega}{2r_j}\frac{\Delta r_{j-1}^2 + \Delta r_j^2}{\Delta r_{j-1} + \Delta r_j}, \omega = 1,$

while $\rho_j, c_j, w_{bl,0,j}$, $q_{m,bas,0,j}$ are obtained from Table 2.3 for neck skin tissue.

Then for the imaginary nodes 18, 35 the skin boundary condition is applied, which is Eq. (4.22), for $j \to 17,34 \; and \; (j+1)^{'} \to 18,35$ respectively.

$$\left[\frac{k_{17}}{r_{sk} \ln\left(\frac{r_{sk}}{r_{17}}\right)} \left(1 - \frac{\ln\left(\frac{r_{sk}}{r_{18}}\right)}{\ln\left(\frac{r_{17}}{r_{18}}\right)} \right) - \frac{\ln\left(\frac{r_{sk}}{r_{18}}\right)}{\ln\left(\frac{r_{17}}{r_{18}}\right) R_{lT}} \right] T_{17} + \left(\frac{\ln\left(\frac{r_{sk}}{r_{17}}\right)}{\ln\left(\frac{r_{17}}{r_{18}}\right) R_{lT}} + \frac{k_{17}}{r_{sk} \ln\left(\frac{r_{17}}{r_{18}}\right)} \right) T_{18} = \frac{p_{sk} - p_{air}}{R_{e,lT}} - \frac{T_o}{R_{lT}}$$

$$\left[\frac{k_{34}}{r_{sk} \ln\left(\frac{r_{sk}}{r_{34}}\right)} \left(1 - \frac{\ln\left(\frac{r_{sk}}{r_{35}}\right)}{\ln\left(\frac{r_{34}}{r_{35}}\right)} \right) - \frac{\ln\left(\frac{r_{sk}}{r_{35}}\right)}{\ln\left(\frac{r_{34}}{r_{35}}\right) R_{lT}} \right] T_{34} + \left(\frac{\ln\left(\frac{r_{sk}}{r_{34}}\right)}{\ln\left(\frac{r_{34}}{r_{35}}\right) R_{lT}} + \frac{k_{34}}{r_{sk} \ln\left(\frac{r_{34}}{r_{35}}\right)} \right) T_{35} = \frac{p_{sk} - p_{air}}{R_{e,lT}} - \frac{T_o}{R_{lT}}$$

with $R_{lT} = 1/(h_c + h_r)$, $R_{e,lT} = 1/(L_a \, h_c)$, $p_{air} = RH \; p_{air,sat}$.

Finally, the linear equation system is completed with the last equation (4.28) applied for the blood pool temperature $T_{bl,p}$ considering only the regular points as

$$\sum_{e}^{1} \left(\frac{\sum_{j}^{34} \beta_{e,j} V_{e,j}}{h_{x,e} + \sum_{j}^{34} \beta_{e,j} V_{e,j}} \cdot \sum_{j}^{34} \beta_{e,j} V_{e,j} T_{e,j} \right) - \sum_{e}^{1} \left(\frac{\left(\sum_{j}^{34} \beta_{e,j} V_{e,j} \right)^2}{h_{x,e} + \sum_{j}^{34} \beta_{e,j} V_{e,j}} \right) T_{bl,p} = 0 .$$

The simulation solves the transient problem with initial element temperatures in both simulations A and B at $40^{o}C$, reaching finally the steady conditions. Again, Simulation B needs more time until it reaches the steady condition compared to Simulation A, as the blood pool temperature is influenced by all node temperatures in every iteration. In Table 5.10 and Table 5.11 the steady state temperatures of the head are presented, while the calculated steady state blood pool temperature is shown in Table 5.11. Furthermore, Figure 5.7 shows the temperatures

for three points in the neck of the transient problem until it reaches steady conditions. The three points are the core node, the node N=7 at r=5.015 cm, which is the last (non-fictitious) muscle node and the skin surface node of the posterior sector. The point on the skin surface it is not a typical mesh node and its temperature is calculated with Eq. (4.11) using information from nodes N=35 and N=35. Finally, the unsteady blood pool temperature is presented for Simulation B in Figure 5.7. The unsteady results give information about the temperature changes that further supports the verification of the present work.

NECK									
$T_{bl,p}$ **imposed at 37** ^oC									
Sector: Anterior					**Sector: Posterior**				
Node	Radius [cm]	Tissue	Temp. [^oC]	Comm.	**Node**	Radius [cm]	Tissue	Temp. [^oC]	Comm.
1	1,9	Bone	37,19	T_{core}	**1**	1,9	Bone	37,19	T_{core}
2	2,79	Bone	37,16	Imaginary	**19**	2,79	Bone	37,16	Imaginary
3	1,455	Muscle	37,23	Imaginary	**20**	1,455	Muscle	37,24	Imaginary
4	2,345	Muscle	37,16		**21**	2,345	Muscle	37,16	
5	3,235	Muscle	37,06		**22**	3,235	Muscle	37,05	
6	4,125	Muscle	36,88		**23**	4,125	Muscle	36,87	
7	5,015	Muscle	36,58		**24**	5,015	Muscle	36,56	
8	5,905	Muscle	36,06	Imaginary	**25**	5,905	Muscle	36,03	Imaginary
9	5,435	Fat	36,35	Imaginary	**26**	5,435	Fat	36,33	Imaginary
10	5,485	Fat	36,28		**27**	5,485	Fat	36,25	
11	5,535	Fat	36,20		**28**	5,535	Fat	36,17	
12	5,585	Fat	36,12	Imaginary	**29**	5,585	Fat	36,09	Imaginary
13	5,546	Skin	36,17	Imaginary	**30**	5,546	Skin	36,14	Imaginary
14	5,574	Skin	36,15		**31**	5,574	Skin	36,12	
15	5,601	Skin	36,14		**32**	5,601	Skin	36,11	
16	5,629	Skin	36,12		**33**	5,629	Skin	36,08	
17	5,656	Skin	36,09		**34**	5,656	Skin	36,06	
18	5,684	Skin	36,06	Imaginary	**35**	5,684	Skin	36,03	Imaginary
	5,67	Skin	36,08	T_{sk}		5,67	Skin	36,04	T_{sk}

Table 5.10 : Steady state temperature distribution of the neck (Simulation A)

NECK									
$T_{bl,p}$ **Part of Solution Procedure**									
Sector: Anterior					**Sector: Posterior**				
Node	Radius [cm]	Tissue	Temp. [^oC]	Comm.	**Node**	Radius [cm]	Tissue	Temp. [^oC]	Comm.
1	1,9	Bone	32,22	T_{core}	1	1,9	Bone		T_{core}
2	2,79	Bone	32,19	Imaginary	19	2,79	Bone	32,19	Imaginary
3	1,455	Muscle	32,26	Imaginary	20	1,455	Muscle	32,26	Imaginary
4	2,345	Muscle	32,19		21	2,345	Muscle	32,19	
5	3,235	Muscle	32,12		22	3,235	Muscle	32,12	
6	4,125	Muscle	32,04		23	4,125	Muscle	32,03	
7	5,015	Muscle	31,90		24	5,015	Muscle	31,89	
8	5,905	Muscle	31,66	Imaginary	25	5,905	Muscle	31,65	Imaginary
9	5,435	Fat	31,79	Imaginary	26	5,435	Fat	31,79	Imaginary
10	5,485	Fat	31,76		27	5,485	Fat	31,75	
11	5,535	Fat	31,72		28	5,535	Fat	31,72	
12	5,585	Fat	31,69	Imaginary	29	5,585	Fat	31,68	Imaginary
13	5,54625	Skin	31,71	Imaginary	30	5,54625	Skin	31,70	Imaginary
14	5,57375	Skin	31,70		31	5,57375	Skin	31,70	
15	5,60125	Skin	31,70		32	5,60125	Skin	31,69	
16	5,62875	Skin	31,69		33	5,62875	Skin	31,68	
17	5,65625	Skin	31,68		34	5,65625	Skin	31,67	
18	5,68375	Skin	31,67	Imaginary	35	5,68375	Skin	31,66	Imaginary
	5,67	Skin	31,67	T_{sk}		5,67	Skin	31,67	T_{sk}
			31,90	$T_{bl,p}$				31,90	$T_{bl,p}$

Table 5.11 : Steady state temperature distribution of the neck (Simulation B)

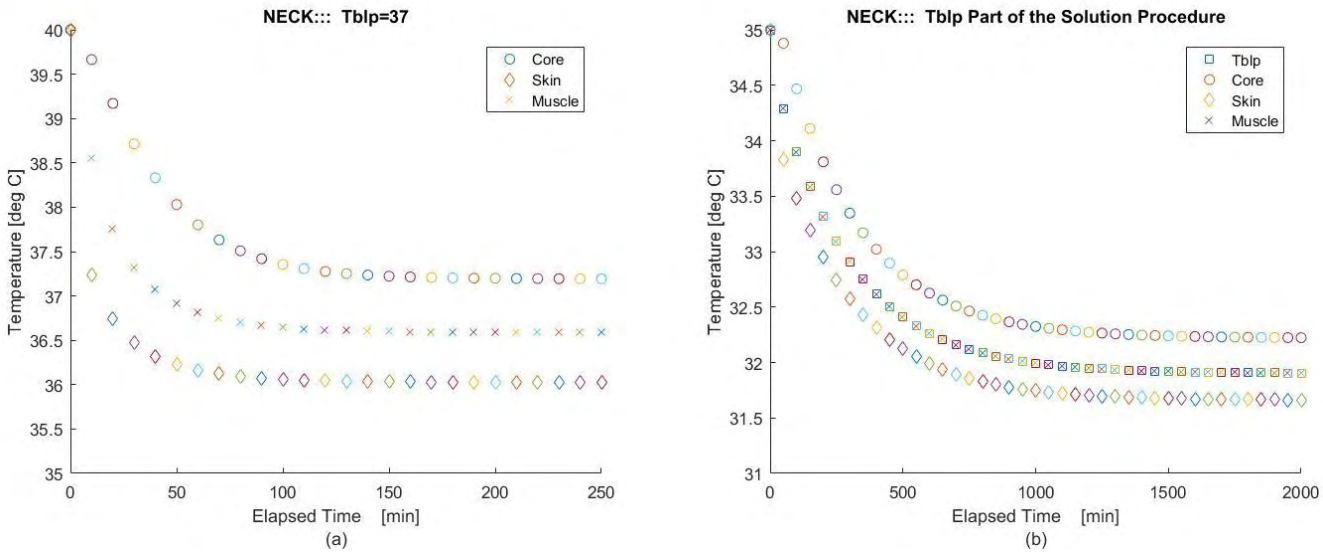

Figure 5.7 : Temperatures at three neck nodes: (a) Simulation A and (b) Simulation B

6 Concluding remarks and future work

The Fiala model has been implemented to develop a Matlab code for simulating human thermoregulation. The computer model simulates the heat transfer within separate human body parts and the heat exchange with the environment considering the passive system. The human body is separated into spherical or cylindrical body parts (elements), which are further separated into spherical or cylindrical tissue layers as well as into sectors. The separation into sectors enables the model to take into consideration the non-uniform environmental conditions taking place around any human body part. Realistic properties of all the human tissues are used and all mechanisms contributing to the heat transfer are considered. They include a) heat conduction within the tissue and between adjacent tissues, b) metabolic heat production, c) blood circulatory system, d) convection, e) long wave radiation, f) short wave irradiation, g) evaporation, h) respiration and i) clothing. The computer model requires the following seven variables as inputs: air temperature and velocity, mean radiant temperature, air humidity, radiation intensity, activity level and the clothing resistances. Then, it calculates the local skin temperatures, the core temperatures and the temperature profile within the tissue all in transient conditions.

For solving the heat transfer problem the finite difference method (FDM) is used. All equations in polar and spherical coordinates are discretized and they are solved implicitly with the Crank Nicholson method. The boundary conditions formulation is also explicitly described for both polar and spherical coordinates.

Two benchmark tests of the developed computer model are carried out in order to verify its accuracy level. These tests concern simulations with simplifications so that different parts of the code can be assessed. The first test simulates a cylindrical element composed of uniform

muscle tissue which initially is at 0^{o}C and then, arterial blood at constant temperature and with constant flow rate is supplied. The second test simulates a spherical element composed of uniform brain tissue which is initially at 37^{o}C and it is exposed to an environment at 0^{o}C, while no blood flows and no metabolic heat is produced. As a result the cylindrical element is heated up to some steady-state conditions, while the spherical element is cooled down to 0^{o}C. In both tests, the temperature distribution rates are compared with corresponding results in the Fiala papers and very good agreement is observed. Furthermore, the spherical head element and the cylindrical neck element in thermal neutral conditions are simulated. In both elements all tissue layers and properties are considered. The obtained temperature distributions are physically justified based on the initial and boundary conditions.

Further work is required with the developed computer model in order to be able to simulate all 15 elements of the human passive system in a coupled manner. Once the proper modeling of the passive system is validated the work may be extended to incorporate the active system. Then, the thermal sensation of a subject will be able to be predicted.

Furthermore, once the modeling of the active system is complete it would be possible to consider and evaluate the thermal state of a motorcyclist during a long ride under hot weather conditions. Several case scenarios of motorcyclist surrounding conditions can be studied. Especially the effect of the air velocity may be investigated with computational fluid dynamics (CFD) which will provide the capability of developing a coupled CFD-thermal comfort model that is going to evaluate the thermal sensation of the driver, predict the rider's ability to keep driving safely and provide the appropriate information and instructions.

References

[1] "Water Vapor and Saturation Pressure in Humid Air," Engineering Toolbox, 2004. [Online]. Available: https://www.engineeringtoolbox.com/water-vapor-saturation-pressure-air-d_689.html. [Accessed 17 June 2019].

[2] T. Austin, "Long-Distance Riding," *Iron Butt,* pp. 63-66, Summer 2010.

[3] P. Broede, G. Jendritzky, D. Fiala and G. Havenith, "The Universal Thermal Climate Index UTCI in operational use," , 2010.

[4] A. Beizaee, S. K. Firth, K. Vadodaria and D. L. Loveday, "Assessing the ability of PMV model in predicting thermal sensation in naturally ventilated buildings in UK," , 2012.

[5] F. Butera, "Standard and adaptive approach for thermal comfort," 20 June 2017. [Online]. Available: https://www.youtube.com/watch?v=SwZ1FEgangE. [Accessed October 2019].

[6] Y. Cheng, J. Niu and N. Gao, "Thermal comfort models: A review and numerical investigation," *Building and Environment,* vol. 47, no. 47, pp. 13-22, 2012.

[7] C. J. Chou, "The Application of Computational Fluid Dynamics to Comfort Modelling," , 2016.

[8] M. F. M. Din, Y. Y. Lee, M. Ponraj, D. R. Ossen, K. Iwao and S. Chelliapan, "Thermal comfort of various building layouts with a proposed discomfort index range for tropical climate," *Journal of Thermal Biology,* vol. 41, no. 1, pp. 6-15, 2014.

[9] N. Djongyang, R. Tchinda and D. Njomo, "Thermal comfort: A review paper," *Renewable & Sustainable Energy Reviews,* vol. 14, no. 9, pp. 2626-2640, 2010.

[10] D. Fiala, "Dynamic Simulation of Human Heat Transfer and Thermal Comfort," , 1998.

[11] D. Fiala, K. J. Lomas and M. Stohrer, "A computer model of human thermoregulation for a wide range of environmental conditions: the passive system," *Journal of Applied Physiology,* vol. 87, no. 5, pp. 1957-1972, 1999.

[12] D. Fiala, G. Havenith, P. Bröde, B. Kampmann and G. Jendritzky, "UTCI-Fiala multi-node model of human heat transfer and temperature regulation.," *International Journal of Biometeorology,* vol. 56, no. 3, pp. 429-441, 2012.

[13] D. Fiala and G. Havenith, "Modelling Human Heat Transfer and Temperature Regulation," , pp. 265-302, 2015.

[14] M. Fu, W. Weng, W. Chen and N. Luo, "Review on modeling heat transfer and thermoregulatory responses in human body.," *Journal of Thermal Biology,* vol. 62, pp. 189-200, 2016.

[15] A. Gagge, J. Stolwijk and J. Hardy, "Comfort and thermal sensations and associated physiological responses at various ambient temperatures," *Environmental Research,* vol. 1, no. 1, pp. 1-20, 1967.

[16] A. Gagge, J. Stolwijk and Y. Nishi, "An Effective Temperature Scale Based on a Simple Model of Human Physiological Regulatiry Response," *Memoirs of the Faculty of Engineering, Hokkaido University = 北海道大学工学部紀要,* vol. 13, pp. 21-36, 1972.

[17] G. Havenith and H. O. Nilsson, "Correction of clothing insulation for movement and wind effects, a meta-analysis," *European Journal of Applied Physiology,* vol. 92, no. 6, pp. 636-640, 2004.

[18] G. Havenith, D. Fiala, K. Błazejczyk, M. Richards, P. Bröde, I. Holmér, H. Rintamaki, Y. Benshabat and G. Jendritzky, "The UTCI-clothing model," *International Journal of Biometeorology,* vol. 56, no. 3, pp. 461-470, 2012.

[19] K. Katić, R. Li and W. Zeiler, "Thermophysiological models and their applications: a review," *Building and Environment,* vol. 106, pp. 286-300, 2016.

[20] W. v. d. Linden, M. Loomans, J. Hensen and M. G. L. C. Loomans, "Adaptive thermal comfort explained by PMV," , 2008.

[21] B. W. Olesen and G. S. Brager, "A Better Way to Predict Comfort: The New ASHRAE Standard 55-2004," *Center for the Built Environment,* 2004.

[22] R. A. Pielke, "Encyclopædia Britannica," [Online]. Available: https://www.britannica.com/science/atmosphere. [Accessed November 2019].

[23] A. Shitzer and R. C. Eberhart, "Heat transfer in medicine and biology : analysis and applications," , 1985.

[24] J. A. J. Stolwijk, "A mathematical model of physiological temperature regulation in man," , 1971.

[25] S. Takada, A. Sasaki and R. Kimura, "Fundamental study of ventilation in air layer in clothing considering real shape of the human body based on CFD analysis," *Building and Environment,* vol. 99, pp. 210-220, 2016.

[26] D. P. Wyon, I. Wyon and F. Norin, "Effects of moderate heat stress on driver vigilance in a moving vehicle," *Ergonomics,* vol. 39, no. 1, pp. 61-75, 1996.

[27] J. Yang, W. Weng, F. Wang and G. Song, "Integrating a human thermoregulatory model with a clothing model to predict core and skin temperatures," *Applied Ergonomics,* vol. 61, pp. 168-177, 2017.

[28] M. Zwolińska, "Case Study of the Impact of Motorcycle Clothing on the Human Body and Its Thermal Insulation," *Fibres & Textiles in Eastern Europe,* 2013.

Appendix A Heat transfer rate in cylindrical and spherical shells

In the absence of work and mass flow, it may be written for a control volume that

$$\dot{Q}_{in} = \dot{Q}_{out} \ . \tag{A.1}$$

Then, in 1D problems, due to energy conservation, it is evident that

$$\frac{d\dot{Q}}{dr} = 0 \Rightarrow \frac{d}{dr}\left(-kA(r)\frac{dT}{dr} \right) = 0 \, . \tag{A.2}$$

For a cylindrical shell with uniform thermal conductivity k in order to calculate the radial heat rate knowing that the shell surface area is $A(r) = \varphi r h$, where h is the cylinder shell height and φ (rad) is the angle of the shell, Eq. (A.2) is integrated to yield

$$\frac{d}{dr}\left(-k\varphi h r\frac{dT}{dr} \right) = 0 \Rightarrow \frac{d}{dr}\left(r\frac{dT}{dr} \right) = 0 \Rightarrow r\frac{dT}{dr} = a \ \Rightarrow \tag{A.3}$$

$$dT = \frac{a}{r}dr \Rightarrow T(r) = a \cdot \ln r + b \tag{A.4}$$

By applying the boundary conditions $T(r_1) = T_1$ and $T(r_2) = T_2$ results to

$$\left\{ \begin{array}{l} a = \dfrac{T_1 - T_2}{\ln\left(\dfrac{r_1}{r_2} \right)} \\ b = \dfrac{T_2 \ln(r_1) - T_1 \ln(r_2)}{\ln\left(\dfrac{r_1}{r_2} \right)} \end{array} \right\} \Rightarrow T(r) = \frac{T_1 \ln\left(\dfrac{r}{r_2} \right) - T_2 \ln\left(\dfrac{r}{r_1} \right)}{\ln\left(\dfrac{r_1}{r_2} \right)} \, . \tag{A.5}$$

Finally, by combining the following equations, the radial heat flow rate for a cylindrical shell is deduced:

$$\left.\begin{aligned} a &= \frac{T_1 - T_2}{\ln\left(\frac{r_1}{r_2}\right)} = r\frac{dT}{dr} \\ \dot{Q} &= -k\,\varphi\, h\, r\frac{dT}{dr} \end{aligned}\right\} \Rightarrow \dot{Q} = -k\,\varphi\, h\frac{T_2 - T_1}{\ln\left(\frac{r_2}{r_1}\right)} \tag{A.6}$$

Similarly, for a spherical shell with uniform thermal conductivity k, the radial heat rate through a shell surface area of $A(r) = 2\varphi r^2$, where φ the angle of the spherical shell, can be found by integrating Eq. (A.2) as

$$\frac{d}{dr}\left(-k\,2\varphi r^2\frac{dT}{dr}\right) = 0 \Rightarrow \frac{d}{dr}\left(r^2\frac{dT}{dr}\right) = 0 \Rightarrow r^2\frac{dT}{dr} = a \Rightarrow \tag{A.7}$$

$$dT = \frac{a}{r^2}dr \Rightarrow T(r) = -\frac{a}{r} + b \tag{A.8}$$

By applying the boundary conditions $T(r_1) = T_1 \; and \; T(r_2) = T_2$ to $T(r) = -\frac{a}{r} + b$ results to

$$\left.\begin{aligned} a &= \frac{T_1 - T_2}{\frac{1}{r_2} - \frac{1}{r_1}} \\ b &= \frac{r_2 T_2 - r_1 T_1}{r_2 - r_1} \end{aligned}\right\} \Rightarrow T(r) = \frac{T_1 - T_2}{\frac{r}{r_1} - \frac{r}{r_2}} + \frac{r_2 T_2 - r_1 T_1}{r_2 - r_1} \tag{A.9}$$

Finally, by combining the following equations the radial heat flow rate for a spherical shell is deduced:

$$\left.\begin{aligned} \dot{Q} &= -k\,2\varphi r^2\frac{dT}{dr} \\ r^2\frac{dT}{dr} &= a \\ a &= \frac{T_1 - T_2}{\frac{1}{r_2} - \frac{1}{r_1}} \end{aligned}\right\} \Rightarrow \dot{Q} = -k\,2\varphi\frac{T_1 - T_2}{\frac{1}{r_2} - \frac{1}{r_1}} \tag{A.10}$$